The International Journal of Advanced Manufacturing Technology (2024) 133:5715–5742
https://doi.org/10.1007/s00170-024-14053-1

ORIGINAL ARTICLE

Chatter-free tool orientations during five-axis ball-end milling of curved thin-walled parts

Wang Dazhen[1,2] · Tian Weijun[3] · Zhou Jinhua[2] · Ren Junxue[2]

Received: 14 September 2023 / Accepted: 20 June 2024 / Published online: 6 July 2024

Abstract
Tool orientation is an important factor for improving machining stability in five-axis milling. However, there is still a lack of tool orientation planning strategy that is applied to the milling of curved thin-walled parts. This paper proposes a process mechanics-based method to optimize tool orientation to suppress chatter during five-axis ball-end milling of thin-walled parts. First, a coupling dynamic model considering both the flexible tool and workpiece is presented in the tool coordinate system, the model can predict the cutting stability of the entire process of milling thin-walled parts. Then, a binary search algorithm-based single-frequency method is presented to calculate limiting cutting depth. The method does not rely on the initial cutting depth and the increment of cutting depth which selected for calculation, the proposed method can expedite the convergence process for calculating the limiting cutting depth. Moreover, an iterative strategy of first generating smooth tool orientations through the representative tool orientations (RTOs) of typical cutter locations (CLs), and then checking the machining stability and adjusting the tool orientations is proposed to generate chatter-free tool orientations along the tool path. A machining stability factor is proposed to select tool orientation, and the tool orientation with a higher value of the machining stability factor is selected as the RTO. The proposed method only needs to obtain the chatter-free tool orientation regions at typical CLs, the calculation process is rapid. The proposed method has been experimentally proven in five-axis ball-end milling of the block workpiece and curved thin-walled part.

Keywords Five-axis · Ball-end milling · Tool orientations · Thin-walled parts · Process mechanics

1 Introduction

Due to the better tool accessibility and the increased flexibility of machining, five-axis milling has been widely used in machining parts with complex sculpture surfaces, such as turbine blades, impellers, and dies. There have been significant researches reported in tool orientation planning and tool path generation, mainly based on geometry, kinematics, and mechanics[1, 2]. Interference and collision are the primary factors that need to be considered in geometrical analysis. Singularity and smoothness are the primary factors that need to be considered in kinematics. The deformation caused by statics and chatter caused by dynamics are the primary factors that need to be considered in mechanics. The neglect of process mechanics may lead to excessive cutting force and chatter, resulting in decreased productivity, and poor surface quality. To overcome this problem, this paper proposes a process mechanics-based method to generate chatter-free tool orientations along the tool path in five-axis ball-end milling of thin-walled parts.

Firstly, the studies of the influence of the tool orientation on the cutter-workpiece engagement (CWE), cutting force, and machining stability will be presented. Then, the research status of the tool orientation optimization based on statistics is described. Moreover, an overview of tool orientation optimization based on dynamics is presented.

Tool orientation in five-axis ball-end milling affects local undeformed chip thickness and CWE, which result in the cutting force and machining stability varying with tool orientation. The study [3] found that both the CWE and cutting force vector varied with the changes in tool orientation. Ozturk et al. [4] investigated the effect of tilt and lead angles on cutting forces, torque, form errors, and stability of five-axis ball-end milling processes. It was shown that the cutting geometry, mechanics, and dynamics vary significantly and

Tian Weijun, Zhou Jinhua, and Ren Junxue contributed equally to this work

Extended author information available on the last page of the article

non-linearly with tool posture. Zhan and Jiang et al. [5] analyzed the effect of tool orientation on the stability prediction of five-axis ball-end milling with variable pitch tools and regular tools. Tang and Peng et al. [6] compared and analyzed the effect of tool orientation on process damping and stability boundary, they found that the increment of critical cutting depth was significantly correlated with the tool orientation. Tang and Zhu et al. [7] investigated the effect of the lead and tilt angles on the critical cutting depth based on stability constraint. Falta et al. [8] proposed an alternative mathematical formulation of the ZOA-based machining stability prediction for 5-axis ball-end milling. They analyzed the influence of lead angle and tilt angle on the cutting force Jacobian and then explained the influence of lead angle and tilt angle on stability. They have not studied the generation of chatter-free tool orientations along the tool path. In addition, the studies [9–12] showed that the lead and tilt angles of tool orientation had a significant effect on the absolute stability limit. Hence, the process mechanics should be considered to optimize tool orientations.

To reduce the cutting force-induced deformation in milling thin-walled parts, Cai et al. [13] proposed a stiffness matching-based algorithm to optimize cutter orientation. Zhang et al. [14] developed an analytical method to calculate the instantaneous CWE conditions by incorporating tool orientation and cutter runout. Then they studied the influence of lead and tilt angles on the maximum cutting force and form error for three kinds of geometrical characteristics. Subsequently, a tool orientation optimization strategy was presented with different constraints in roughing and finishing for the plane, cylindrical, and spherical surfaces. Yigit et al. [15] proposed a mechanics-based approach to select the tool postures for five-axis ball-end milling of flexible parts, the proposed method involved cutting force, torque, vibration, and surface quality. However, the papers [13–15] only considered the influence of static cutting force, but they did not consider the influence of dynamic cutting force.

Although numerous researches on machining stability have been presented as described in the paper [16], there has been a very limited effort reported in optimizing the tool orientation to avoid chatter. Tunc et al. [17] proposed a process simulation integrated tool orientation selection approach to adjust the tool orientation along an already generated five-axis milling path for improved process in terms of cutting forces, stability, and machine tool motion. Wang et al. [18] constructed the posture stability graphs to select chatter-free cutter postures. In addition, Sun and Altintas [19] modelled the stability of five-axis ball-end milling, and they searched the chatter-free tool orientations using the Nyquist criterion. Then, they adjusted the tool orientation to avoid chatter along the tool path. Zhao and Wang et al. [20] constructed the posture accessibility and stability diagram (PASD) by identifying interference- and chatter-free cutter postures based on geometric analysis and machining dynamic analysis. Also, they analyzed the relationship between surface roughness and maximum cutter deformation force and proposed a surface roughness prediction model. Then, based on the proposed PASD and surface roughness prediction model, they proposed a cutter posture optimization algorithm to minimize surface roughness. However, in the papers [17–19], the regions of chatter-free tool orientation at each cutter location (CL) point should be obtained, the efficiency may be limited. To achieve a balance between the smooth tool orientations and suppression of chatter and surface location error, Huang et al. [21] presented a minimax optimization approach for planning tool orientations. This method did not need to get the regions of chatter-free tool orientation at each CL point in advance.

The studies [17–21] focused on the milling of rigid workpiece. The paper [11] studied the influence of lead and tilt angles on the stability limits during five-axis milling thin-walled workpiece, however, this paper did not propose a strategy to generate chatter-free and smooth tool orientations along the tool path. Karimi and Altintas [22] studied the effects of tool orientation on the cutting stability and forced vibration through simulations. Then tool orientation was optimized to mitigate chatter and forced vibration problems caused by the high flexibilities of thin-walled blades and slender cutting tools in five-axis ball-end milling operations. However, in the reference [22] the thickness of the thin-walled blades is 8 mm which is too thick. There is still a lack of efficient tool orientation planning strategy that is applied to the milling of curved thin-walled parts. The milling of thin-walled parts is more complicated than the milling of rigid parts. During the milling of thin-walled parts, the material removal causes a change in workpiece dynamics. Moreover, the change of local workpiece dynamics along the tool path will change the machining system from a flexible workpiece to a flexible tool. In the process of machining the free end of the workpiece, the workpiece is the flexible body, while in the process of machining the fixed end of the workpiece, the tool is the flexible body.

In this paper, a tool orientation optimization method is presented to generate a chatter-free tool path in the five-axis ball-end milling of curved thin-walled parts. To improve calculation efficiency, a binary search algorithm-based method is proposed to calculate limiting cutting depth for milling of thin-walled parts. A dynamic model considering both the flexible tool and workpiece is modeled in the tool coordinate system. Moreover, an iterative strategy of first generating the

smooth tool orientations through the representative tool orientations (RTOs), and then checking the machining stability and adjusting the tool orientation is proposed to optimize tool orientation. A machining stability factor is proposed to select tool orientation, the tool orientation with a higher value of machining stability factor is selected as the RTO. The effectiveness of the presented method has been experimentally verified in the five-axis ball-end milling of the block workpiece and the curved thin-walled part.

The paper is organized as follows. In Section 2, the process coordinate systems and the transformations between these coordinate systems are defined. In Section 3, the stability prediction model for the milling thin-walled part is constructed. In Section 4, the tool orientation optimizing and smoothing strategy is proposed. In Section 5, simulations and tests are carried out to verify the effectiveness of the proposed method.

2 Definition of process coordinate systems and transformations

The configuration for the table-tilting type five-axis machine tool is shown in Fig. 1a, θ_B, and θ_C are the rotation angles of the B and C axes of the machine tool, respectively. In order to illustrate the calculation process, four coordinate systems are defined, namely, machine coordinate system (MCS), feed coordinate system (FCS), workpiece coordinate system (WCS), and tool coordinate system (TCS). In the FCS, $\boldsymbol{F}$ is the feed direction, $\boldsymbol{C}$ is the cross-feed direction, and $\boldsymbol{N}$ is the surface normal direction of the workpiece. The lead angle is defined as the angular rotation of the tool axis about $\boldsymbol{C}$, and the tilt angle is defined as the angular rotation of the tool axis about $\boldsymbol{F}$.

The surface normal $\boldsymbol{N}$ can be obtained by setting the lead and tilt angles to be zero in the process of generating the CL file by CAD/CAM software, the surface normal is coincident with the tool orientation in the CL file, and the CL point is equal to the cutter contact (CC) point. The feed direction $\boldsymbol{F}$ can be expressed as follows:

$$\boldsymbol{F} = \frac{(x_{p+1} - x_p, y_{p+1} - y_p, z_{p+1} - z_p)}{\sqrt{(x_{p+1} - x_p)^2 + (y_{p+1} - y_p)^2 + (z_{p+1} - z_p)^2}} \tag{1}$$

where (x_p, y_p, z_p) and $(x_{p+1}, y_{p+1}, z_{p+1})$ are the coordinates of the two consecutive CC points. The cross-feed direction $\boldsymbol{C}$ is generated by the cross product of $\boldsymbol{N}$ and $\boldsymbol{F}$. For the lead angle α and tilt angle β, the tool orientation with respect to WCS can be obtained as follows:

$$\boldsymbol{A}(\alpha, \beta) = \boldsymbol{R}(\boldsymbol{C}, \alpha)\boldsymbol{R}(\boldsymbol{F}, \beta)\boldsymbol{N} \tag{2}$$

The expressions of $\boldsymbol{R}(\boldsymbol{C}, \alpha)$ and $\boldsymbol{R}(\boldsymbol{F}, \beta)$ are shown in Appendix.

The CL point is written as follows:

$$CL(\alpha, \beta) = CC + R_0(\boldsymbol{N} - \boldsymbol{A}(\boldsymbol{\alpha}, \boldsymbol{\beta})) \tag{3}$$

where R is the radius of the tool. The axis directions of TCS are defined as follows:

$$\begin{cases} \boldsymbol{z}_T(\alpha, \beta) = \boldsymbol{A}(\alpha, \beta)/|\boldsymbol{A}(\alpha, \beta)| \\ \boldsymbol{y}_T(\alpha, \beta) = (\boldsymbol{A}(\alpha, \beta) \times \boldsymbol{F})/|\boldsymbol{A}(\alpha, \beta) \times \boldsymbol{F}|, \boldsymbol{A}(\alpha, \beta) \times \boldsymbol{F} \neq \boldsymbol{0} \\ \boldsymbol{x}_T(\alpha, \beta) = \boldsymbol{y}_T(\alpha, \beta) \times \boldsymbol{z}_T(\alpha, \beta) \end{cases} \tag{4}$$

The frequency response functions (FRFs) of the workpiece are measured in WCS, and the FRFs of the tool are measured in MCS, however, the cutting force is calculated in TCS. Thus, the transformations between WCS, MCS, and TCS should be constructed, and the stability of the machining system should be analyzed in TCS. The rotation matrix from TCS to WCS can be defined as:

$${}^{W}_{T}\boldsymbol{R}(\alpha, \beta) = [\boldsymbol{x}_T(\alpha, \beta), \boldsymbol{y}_T(\alpha, \beta), \boldsymbol{z}_T(\alpha, \beta)] \tag{5}$$

In this paper, when the rotation angles of the B and C axes of the machine tool are zero, the WCS is not aligned with the MCS, and the rotation matrix from MCS to WCS is written as:

$${}^{W}_{M}\boldsymbol{R}_0 = \begin{bmatrix} 0 & 1 & 0 \\ -1 & 0 & 0 \\ 0 & 0 & 1 \end{bmatrix} \tag{6}$$

For the machine tool used in this paper, the tool orientation in CL file can be expressed as a function of θ_B and θ_C:

$$\begin{aligned} \boldsymbol{A}(\alpha, \beta) &= \begin{bmatrix} i(\alpha, \beta) \\ j(\alpha, \beta) \\ k(\alpha, \beta) \end{bmatrix} = {}^{W}_{M}\boldsymbol{R_0}\boldsymbol{R}_z(\theta_C)\boldsymbol{R}_y(\theta_B)\boldsymbol{A}^M \\ &= \begin{bmatrix} 0 & 1 & 0 \\ -1 & 0 & 0 \\ 0 & 0 & 1 \end{bmatrix} \begin{bmatrix} \cos\theta_C & -\sin\theta_C & 0 \\ \sin\theta_C & \cos\theta_C & 0 \\ 0 & 0 & 1 \end{bmatrix} \\ &\quad \begin{bmatrix} \cos\theta_B & 0 & \sin\theta_B \\ 0 & 1 & 0 \\ -\sin\theta_B & 0 & \cos\theta_B \end{bmatrix} \begin{bmatrix} 0 \\ 0 \\ 1 \end{bmatrix} \\ &= \begin{bmatrix} \sin\theta_C \sin\theta_B \\ -\cos\theta_C \sin\theta_B \\ \cos\theta_B \end{bmatrix} \end{aligned} \tag{7}$$

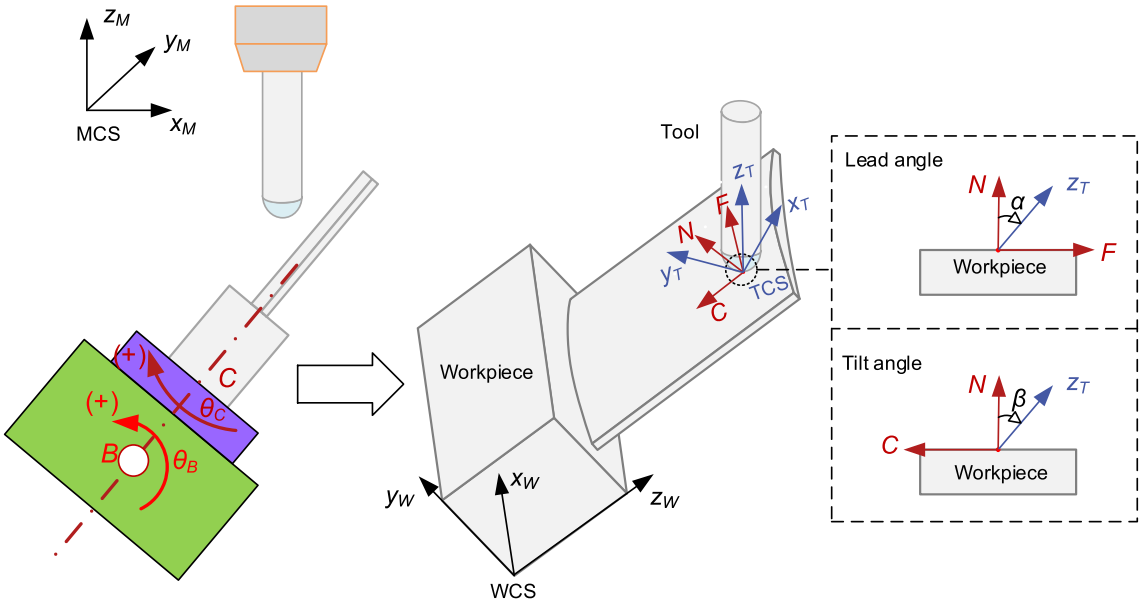

(a)

	i<0	i=0	i>0
j<0	θ_B=arccos(k),θ_C=-arctan(i/j)		
	θ_B=-arccos(k),θ_C=-arctan(i/j)+π	θ_B=-arccos(k),θ_C=-arctan(i/j)+π	θ_B=-arccos(k),θ_C=-arctan(i/j)-π
j=0	θ_B=arccos(k),θ_C=-π/2	Singularity point	θ_B=arccos(k),θ_C=π/2
	θ_B=-arccos(k),θ_C=π/2		θ_B=-arccos(k),θ_C=-π/2
j>0	θ_B=arccos(k),θ_C=-arctan(i/j)-π	θ_B=arccos(k),θ_C=-arctan(i/j)-π	θ_B=arccos(k),θ_C=-arctan(i/j)+π
	θ_B=-arccos(k),θ_C=-arctan(i/j)		

Solutions of (θ_B,θ_C): red color, θ_B>0 ; blue color, θ_B<0

i, j, k represent the components of the tool axis vector along the *x, y*, and *z* axes

(b)

Fig. 1 **a** Configuration for table-tilting five-axis machine tool, workpiece coordinate system (WCS), tool coordinate system (TCS), feed coordinate system (FCS), lead angle, and tilt angle of tool axis; and **b** the solution subspaces of (θ_B, θ_C)

where $\boldsymbol{A}^M$ is the tool orientation with respect to MCS. Then:

$$\cos\theta_B = k(\alpha,\beta), \quad \tan\theta_C = -i(\alpha,\beta)/j(\alpha,\beta) \tag{8}$$

The two solution subspaces of (θ_B, θ_C) are given in Fig. 1b. After the rotational angles θ_B and θ_C are obtained, the transformation matrix from MCS to WCS can be written as:

$$\begin{aligned} {}^W_M\boldsymbol{R}(\alpha,\beta) &= {}^W_M\boldsymbol{R}_0\boldsymbol{R}_z(\theta_C)\boldsymbol{R}_y(\theta_B) \\ &= \begin{bmatrix} \sin\theta_C\cos\theta_B & \cos\theta_C & \sin\theta_C\sin\theta_B \\ -\cos\theta_C\cos\theta_B & \sin\theta_C & -\cos\theta_C\sin\theta_B \\ -\sin\theta_B & 0 & \cos\theta_B \end{bmatrix} \end{aligned} \tag{9}$$

The transformation matrix from TCS to MCS can be written as:

$${}^M_T\boldsymbol{R}(\alpha,\beta) = {}^W_M\boldsymbol{R}^{-1}(\alpha,\beta){}^W_T\boldsymbol{R}(\alpha,\beta), {}^M_W\boldsymbol{R}(\alpha,\beta) = {}^W_M\boldsymbol{R}^{-1}(\alpha,\beta) \tag{10}$$

where ${}^W_M\boldsymbol{R}^{-1}(\alpha,\beta)$ is the inverse matrix of ${}^W_M\boldsymbol{R}(\alpha,\beta)$.

3 Predicting stability for five-axis ball-end milling of thin-walled part

Ozturk and Budak [10] proposed an iterative method to calculate stability limits. The iteration was performed by incrementing the cutting depth of Δa until all the calculated limiting cutting depths were less than the cutting depth in the analysis. However, if an improper value is selected as the initial cutting depth, and the value of limiting cutting depth is great, this method is inefficient. Moreover, in industry practice, the acceptable chatter-free cutting parameters is often ensured by the lobe's outer contour, which is also a single-valued function of spindle speed [23]. Hence, to improve calculation efficiency, a binary search algorithm-based single-frequency method is adopted to calculate limiting cutting depth. The iteration process for calculating limiting cutting depth b is described as follows:

1. Select a small cutting depth a_1 and calculate the CWE, the calculated limiting cutting depth is b_1, select the minimum cutting depth a_2 which is greater than b_1.
2. Set $L = a_1$, $U = a_2$, $M = (a_1 + a_2)/2$, the allowance error $\epsilon = 1 \times 10^{-2}$ mm; for the cutting depth M, the calculated limiting cutting depth is B, and $a_1 < B < a_2$.
3. Compare M and B:
   (a) if $B < M$ and $M - B < \epsilon$, then $b = B$;
   (b) if $B < M$ and $M - B > \epsilon$, set $U = M$, if $B > L$, set $L = B$, then $M = (L + U)/2$, for the cutting depth M, calculate the limiting cutting depth B, go to step 3;
   (c) if $B > M$ and $B - M < \epsilon$, then $b = B$;
   (d) if $B > M$ and $B - M > \epsilon$, set $L = M$, if $U > B$, set $U = B$, then $M = (L + U)/2$, for the cutting depth M, calculate the limiting cutting depth B, go to step 3.

Next, the expression for limiting cutting depth will be presented. Generally, during finishing milling of thin-walled parts, the tool is regarded as a rigid body compared with the flexible workpiece [24]. However, for cantilever-shaped structures, as the cutter advances from the free end of the workpiece to the fixed end, the machining system will change from flexible workpiece and flexible tool to rigid workpiece and flexible tool as shown in Fig. 2. Both the flexible tool and flexible workpiece should be considered. To describe the calculation process conveniently, the tool paths are marked by *curve h* as shown in Fig. 2, where h is the distance from the cutting position to the upper surface of the part along the z direction, the unit is mm.

For ball-end milling, the dynamic cutting force acting on the lth disk can be expressed as:

$$\left[F^d_{l,x,y,z}(x,z,\alpha,\beta,t)\right] = \Delta z\boldsymbol{A}_l(x,z,\alpha,\beta,t)\left[\Delta^T(x,z,\alpha,\beta,t)\right] \tag{11}$$

with

$$\begin{aligned} \left[\Delta^T(x,z,\alpha,\beta,t)\right] = &\left(\begin{bmatrix} x^T_T(x,z,\alpha,\beta,t) \\ y^T_T(x,z,\alpha,\beta,t) \\ z^T_T(x,z,\alpha,\beta,t) \end{bmatrix} - \begin{bmatrix} x^T_W(x,z,\alpha,\beta,t) \\ y^T_W(x,z,\alpha,\beta,t) \\ z^T_W(x,z,\alpha,\beta,t) \end{bmatrix}\right) \\ &- \left(\begin{bmatrix} x^T_T(x,z,\alpha,\beta,t-\tau) \\ y^T_T(x,z,\alpha,\beta,t-\tau) \\ z^T_T(x,z,\alpha,\beta,t-\tau) \end{bmatrix} - \begin{bmatrix} x^T_W(x,z,\alpha,\beta,t-\tau) \\ y^T_W(x,z,\alpha,\beta,t-\tau) \\ z^T_W(x,z,\alpha,\beta,t-\tau) \end{bmatrix}\right) \end{aligned} \tag{12}$$

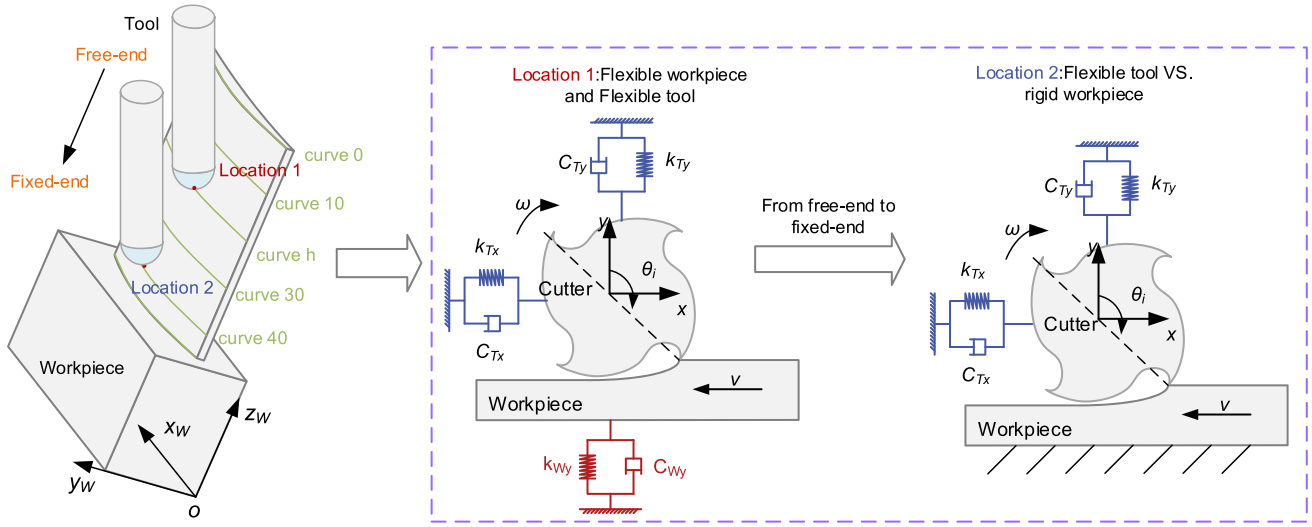

Fig. 2 Evolution of machining system as cutter advances from free-end to fixed-end

where $(x_T^T(t), y_T^T(t), z_T^T(t))^T$ and $(x_W^T(t), y_W^T(t), z_W^T(t))^T$ represent the dynamic displacements of the tool and workpiece at present tooth period in TCS frame, $(x_T^T(t-\tau), y_T^T(t-\tau), z_T^T(t-\tau))^T$ and $(x_W^T(t-\tau), y_W^T(t-\tau), z_W^T(t-\tau))^T$ represent the dynamic displacements of the tool and workpiece at previous tooth period, Δz is the height of the disk, $\boldsymbol{A}_l(x,z,\alpha,\beta,t)$ is the directional coefficient matrix. When the single-frequency method [25] is adopted to calculate the limiting cutting depth, the average component of the Fourier series expansion is adopted to represent $[A(t)]$, then:

$$\left[F_{l,x,y,z}^d(x,z,\alpha,\beta,t)\right] = \Delta z \boldsymbol{A}_{l,0}(x,z,\alpha,\beta)\left[\Delta^T(x,z,\alpha,\beta,t)\right] \tag{13}$$

where

$$\begin{cases} \Delta z = \dfrac{\Delta a}{\cos\gamma(\alpha,\beta)}, \quad \gamma(\alpha,\beta) = \cos^{-1}\left(\dfrac{\boldsymbol{N}\cdot\boldsymbol{A}(\alpha,\beta)}{\sqrt{|\boldsymbol{N}||\boldsymbol{A}(\alpha,\beta)|}}\right) \\ \boldsymbol{A}_{l,0}(x,z,\alpha,\beta) = \dfrac{N}{2\pi}\begin{bmatrix} \alpha_{l,xx}^0(x,z,\alpha,\beta) & \alpha_{l,xy}^0(x,z,\alpha,\beta) & \alpha_{l,xz}^0(x,z,\alpha,\beta) \\ \alpha_{l,yx}^0(x,z,\alpha,\beta) & \alpha_{l,yy}^0(x,z,\alpha,\beta) & \alpha_{l,yz}^0(x,z,\alpha,\beta) \\ \alpha_{l,zx}^0(x,z,\alpha,\beta) & \alpha_{l,zy}^0(x,z,\alpha,\beta) & \alpha_{l,zz}^0(x,z,\alpha,\beta) \end{bmatrix} \end{cases} \tag{14}$$

where

$$\begin{cases} \alpha_{l,xx}^0 = \dfrac{1}{4}\left[K_{l,tc}\cos 2\theta - K_{l,rc}(\sin\kappa_l)(2\theta - \sin 2\theta) - K_{l,ac}(\cos\kappa_l)(2\theta - \sin 2\theta)\right]|_{\theta_{l,st}}^{\theta_{l,ex}} \\ \alpha_{l,xy}^0 = \dfrac{1}{4}\left[-K_{l,tc}(2\theta + \sin 2\theta) + K_{l,rc}\sin\kappa_l\cos 2\theta + K_{l,ac}\cos\kappa_l\cos 2\theta\right]|_{\theta_{l,st}}^{\theta_{l,ex}} \\ \alpha_{l,xz}^0 = \dfrac{1}{2}\left[2K_{l,tc}\cot\kappa_l\sin\theta - 2K_{l,rc}\cos\kappa_l\cos\theta - 2K_{l,ac}\cos\kappa_l\cot\kappa_l\cos\theta\right]|_{\theta_{l,st}}^{\theta_{l,ex}} \end{cases} \tag{15a}$$

$$\begin{cases} \alpha_{l,yx}^0 = \dfrac{1}{4}\left[K_{l,tc}(2\theta - \sin 2\theta) + K_{l,rc}\sin\kappa_l\cos 2\theta + K_{l,ac}\cos\kappa_l\cos 2\theta\right]|_{\theta_{l,st}}^{\theta_{l,ex}} \\ \alpha_{l,yy}^0 = \dfrac{1}{4}\left[-K_{tc}\cos 2\theta - K_{l,rc}(\sin\kappa_l)(2\theta + \sin 2\theta) - K_{l,ac}(\cos\kappa_l)(2\theta + \sin 2\theta)\right]|_{\theta_{l,st}}^{\theta_{l,ex}} \\ \alpha_{l,yz}^0 = \dfrac{1}{2}\left[2K_{l,tc}\cot\kappa_l\cos\theta + 2K_{l,rc}\cos\kappa_l\sin\theta + 2K_{l,ac}\cos\kappa_l\cot\kappa_l\sin\theta)\right]|_{\theta_{l,st}}^{\theta_{l,ex}} \end{cases} \tag{15b}$$

$$\begin{cases} \alpha_{l,zx}^{0} = \left[-K_{l,rc}\cos\kappa_l\cos\theta + K_{l,ac}\sin\kappa_l\cos\theta\right]|_{\theta_{l,st}}^{\theta_{l,ex}} \\ \alpha_{l,zy}^{0} = \left[K_{l,rc}\cos\kappa_l\sin\theta - K_{l,ac}\sin\kappa_l\sin\theta\right]|_{\theta_{l,st}}^{\theta_{l,ex}} \\ \alpha_{l,zz}^{0} = \left[\left(-K_{l,rc}\cos\kappa_l\cot\kappa_l + K_{l,ac}\cos\kappa_l\right)\theta\right]|_{\theta_{l,st}}^{\theta_{l,ex}} \end{cases} \tag{15c}$$

where K_{tc}, K_{rc}, K_{ac} are the cutting force coefficients, they are calibrated by the method proposed in [26]; $\theta_{l,st}$ and $\theta_{l,ex}$ are engagement angles (start and exit angles) for the lth discrete slice, they are calculated by the triple dexel based method presented in [26].

According to Eq. 13, the dynamics of the system in the frequency domain can be expressed as

$$\begin{aligned} \left[F_{x,y,z}^{d}(x,z,\alpha,\beta,i\omega)\right] &= \frac{\Delta a}{\cos\gamma}\left(\sum_{l=1}^{m}\boldsymbol{A}_{l,0}(x,z,\alpha,\beta)\right)\left[\Delta^{T}(x,z,\alpha,\beta,i\omega)\right] \\ &= \frac{\Delta a}{\cos\gamma}\left(\sum_{l=1}^{m}\boldsymbol{A}_{l,0}(x,z,\alpha,\beta)\right)(1-e^{-i\omega\tau}) \\ &\quad \boldsymbol{\Phi}_{TW}^{T}(x,z,\alpha,\beta,i\omega)\left[F_{x,y,z}^{d}(x,z,\alpha,\beta,i\omega)\right] \end{aligned} \tag{16}$$

where m is the number of the disk along the tool axis; $\Phi_{TW}^{T}(i\omega)$ is the relative FRF between the tool and workpiece in TCS, it can be written as:

$$\begin{aligned} &\boldsymbol{\Phi}_{TW}^{T}(x,z,\alpha,\beta,i\omega) = ({}_{T}^{W}\boldsymbol{R}(\alpha,\beta))^{-1}\boldsymbol{\Phi}_{W}^{W}(x,z,i\omega){}_{T}^{W}\boldsymbol{R}(\alpha,\beta) \\ &+({}_{T}^{W}\boldsymbol{R}(\alpha,\beta))^{-1}({}_{W}^{M}\boldsymbol{R}(\alpha,\beta))^{-1}\boldsymbol{\Phi}_{T}^{M}(i\omega){}_{W}^{M}\boldsymbol{R}(\alpha,\beta){}_{T}^{W}\boldsymbol{R}(\alpha,\beta) \end{aligned} \tag{17}$$

where $\omega_{n,W,j}$ is the jth order natural frequency of workpiece; $\xi_{w,j}$ is the jth order damping ratio of workpiece; $\phi_{W,x,q,j}$, $\phi_{W,y,q,j}$, $\phi_{W,z,q,j}$ are the component of jth order modal shape at point q; ω is the frequency of excitation. For the machine tool, the FRFs correspond to the most flexible points PX1 and PY1 (Fig. 5) are written as follows:

$$\boldsymbol{\Phi}_{T}^{M}(i\omega) = \begin{bmatrix} \Phi_{T,xx}^{M}(i\omega) & 0 & 0 \\ 0 & \Phi_{T,yy}^{M}(i\omega) & 0 \\ 0 & 0 & 0 \end{bmatrix} \tag{20}$$

with

$$\begin{cases} \Phi_{T,xx}^{M}(i\omega) = \sum_{j=1}^{n}\dfrac{\left(\phi_{T,x,PX1,j}\right)^{2}}{\omega_{n,T,x,j}^{2} - \omega^{2} + i2\xi_{T,x,j}\omega_{n,T,x,j}\omega} \\ \Phi_{T,yy}^{M}(i\omega) = \sum_{j=1}^{n}\dfrac{\left(\phi_{T,y,PY1,j}\right)^{2}}{\omega_{n,T,y,j}^{2} - \omega^{2} + i2\xi_{T,y,j}\omega_{n,T,y,j}\omega} \end{cases} \tag{21}$$

where $\phi_{T,x,j}$ and $\phi_{T,y,j}$ are the jth order modal shapes of tool in x and y directions, respectively; $\omega_{n,T,x,j}$ and $\omega_{n,T,x,j}$ are the jth order natural frequency of tool in x and y directions, respectively; $\xi_{T,x,j}$ and $\xi_{T,y,j}$ are the jth order damping ratio of tool in x and y directions, respectively; ω is the frequency of excitation.

Equation 16 has nontrivial solutions if the following determinant is equal to zero:

$$\det|\boldsymbol{I} - \lambda(x,z,\alpha,\beta,i\omega)\boldsymbol{\Phi}(x,z,\alpha,\beta,i\omega)| = 0 \tag{22}$$

with

$$\begin{cases} \lambda(x,z,\alpha,\beta,i\omega) = \dfrac{\Delta a(x,z,\alpha,\beta,i\omega)}{\cos\gamma(\alpha,\beta)}\left(1-e^{-i\omega\tau}\right) = \lambda_R(x,z,\alpha,\beta,i\omega) + i\lambda_I(x,z,\alpha,\beta,i\omega) \\ \boldsymbol{\Phi}(x,z,\alpha,\beta,i\omega) = \begin{bmatrix} \Phi_{xx}(x,z,\alpha,\beta,i\omega) & \Phi_{xy}(x,z,\alpha,\beta,i\omega) & \Phi_{xz}(x,z,\alpha,\beta,i\omega) \\ \Phi_{yx}(x,z,\alpha,\beta,i\omega) & \Phi_{yy}(x,z,\alpha,\beta,i\omega) & \Phi_{yz}(x,z,\alpha,\beta,i\omega) \\ \Phi_{zx}(x,z,\alpha,\beta,i\omega) & \Phi_{zy}(x,z,\alpha,\beta,i\omega) & \Phi_{zz}(x,z,\alpha,\beta,i\omega) \end{bmatrix} \\ = \left(\sum_{l=1}^{m}\boldsymbol{A}_{l,0}(x,z,\alpha,\beta)\right)\boldsymbol{\Phi}_{TW}^{T}(x,z,\alpha,\beta,i\omega) \end{cases} \tag{23}$$

where $\boldsymbol{\Phi}_{W}^{W}(x,z,i\omega)$ is the FRF of the workpiece in WCS, $\boldsymbol{\Phi}_{T}^{M}(i\omega)$ is the FRF of the machine tool in MCS. When the cross FRFs are omitted, and only the direct FRFs are considered, the direct FRFs of the workpiece at point q can be expressed as follows:

$$\boldsymbol{\Phi}_{W}^{W}(x,z,i\omega) = \begin{bmatrix} \Phi_{W,x}^{qq}(x,z,i\omega) & 0 & 0 \\ 0 & \Phi_{W,y}^{qq}(x,z,i\omega) & 0 \\ 0 & 0 & \Phi_{W,z}^{qq}(x,z,i\omega) \end{bmatrix} \tag{18}$$

with

$$\begin{cases} \Phi_{W,x}^{qq}(x,z,i\omega) = \sum_{j=1}^{n}\dfrac{(\phi_{W,x,q,j}(x,z))^{2}}{\omega_{n,W,j}^{2} - \omega^{2} + i2\xi_{W,j}\omega_{n,W,j}\omega} \\ \Phi_{W,y}^{qq}(x,z,i\omega) = \sum_{j=1}^{n}\dfrac{(\phi_{W,y,q,j}(x,z))^{2}}{\omega_{n,W,j}^{2} - \omega^{2} + i2\xi_{W,j}\omega_{n,W,j}\omega} \\ \Phi_{W,z}^{qq}(x,z,i\omega) = \sum_{j=1}^{n}\dfrac{(\phi_{W,z,q,j}(x,z))^{2}}{\omega_{n,W,j}^{2} - \omega^{2} + i2\xi_{W,j}\omega_{n,W,j}\omega} \end{cases} \tag{19}$$

Since the size of the matrix $\boldsymbol{\Phi}(x,z,\alpha,\beta,i\omega)$ is 3×3, the solution of Eq. 22 has three different eigenvalues for each frequency ω. For each eigenvalue, the limiting cutting depth is calculated, and the eigenvalue that results in the minimum positive limiting depth is used in the stability diagrams. Defining $\kappa(x,z,\alpha,\beta,i\omega) = \lambda_I(x,z,\alpha,\beta,i\omega)/\lambda_R(x,z,\alpha,\beta,i\omega)$, for the CL point q, the elemental critical depth Δa_{lim} and the limiting cutting depth $a_{\lim}$ can be written as follows:

$$\begin{cases} \Delta a_{\lim}(x,z,\alpha,\beta,i\omega) = \dfrac{1}{2}\lambda_R(x,z,\alpha,\beta,i\omega) \\ (1+\kappa^{2}(x,z,\alpha,\beta,i\omega))\cos\gamma(\alpha,\beta) \\ a_{\lim}(x,z,\alpha,\beta,i\omega) = m\Delta a_{\lim}(x,z,\alpha,\beta,i\omega) \end{cases} \tag{24}$$

The corresponding spindle speed n_s can be written as follows:

$$n_s(x,z,\alpha,\beta,i\omega) = \frac{60\omega}{N\left[(2k+1)\pi - 2\arctan\kappa(x,z,\alpha,\beta,i\omega)\right]} \tag{25}$$

Compared with the iterative method presented in [10], which calculated the limiting cutting depth by incrementing the cutting depth of Δa until all the calculated limiting cutting depths were less than the cutting depth in the analysis, the binary search algorithm based method presented in this paper is efficient.

4 Tool orientation optimizing strategy

This section provides an efficient method to optimize tool orientation to suppress chatter during the five-axis milling process. It is supposed that the interference-free tool path has been already determined by a commercial CAM system.

The basic idea of the proposed method is to proceed iteratively by first generating the smooth tool orientations, and then checking the machining stability and adjusting tool orientations, the method contains three steps. The first step is to assign initial RTOs at crucial areas based on process mechanics. The second step is to interpolate smooth tool orientations at general areas from the RTOs by the quaternion interpolation (QI) algorithm. The third step is to check machining stability at each CL point, if chatter occurs, the chatter-free tool orientation is selected and added to the RTOs. Then, back to the second step to interpolate new tool orientations. This process is repeated until all tool orientations along the tool path are chatter-free.

After the crucial CL points are selected, the chatter-free tool orientations at each crucial CL point are obtained using the Nyquist criterion [27]. According to Eq. 22, the characteristic equation of the system can be rewritten as:

$$
\begin{aligned}
&[1-\Delta z(1-\cos\omega\tau+i\sin\omega\tau)\Phi_{xx}(i\omega)]\times\left\{\begin{array}{l}[1-\Delta z(1-\cos\omega\tau+i\sin\omega\tau)\Phi_{yy}(i\omega)]\\ \times[1-\Delta z(1-\cos\omega\tau+i\sin\omega\tau)\Phi_{zz}(i\omega)]\\ -\Delta z^2(1-\cos\omega\tau+i\sin\omega\tau)^2\Phi_{yz}(i\omega)\Phi_{zy}(i\omega)\end{array}\right\}\\
&+[\Delta z(1-\cos\omega\tau+i\sin\omega\tau)\Phi_{xy}(i\omega)]\times\left\{\begin{array}{l}[-\Delta z(1-\cos\omega\tau+i\sin\omega\tau)\Phi_{yx}(i\omega)]\\ \times[1-\Delta z(1-\cos\omega\tau+i\sin\omega\tau)\Phi_{zz}(i\omega)]\\ -\Delta z^2(1-\cos\omega\tau+i\sin\omega\tau)^2\Phi_{yz}(i\omega)\Phi_{zx}(i\omega)\end{array}\right\}\\
&-[\Delta z(1-\cos\omega\tau+i\sin\omega\tau)\Phi_{xz}(i\omega)]\times\left\{\begin{array}{l}[\Delta z(1-\cos\omega\tau+i\sin\omega\tau)\Phi_{zx}(i\omega)]\\ \times[1-\Delta z(1-\cos\omega\tau+i\sin\omega\tau)\Phi_{yy}(i\omega)]\\ +\Delta z^2(1-\cos\omega\tau+i\sin\omega\tau)^2\Phi_{yx}(i\omega)\Phi_{zy}(i\omega)\end{array}\right\}=0
\end{aligned}
\tag{26}
$$

The stability can be investigated by separating the characteristic equation of the system into real and imaginary parts and plotting its real and imaginary parts on a complex plane. Since the characteristic equation represents the closed-loop system, the process is stable if the polar plot does not encircle the origin.

In the papers [18, 19], for the given spindle speed and cutting depth, the cutter postures are divided into stable and chatter zones by Nyquist stability criteria and Floquet theory, respectively. However, due to the errors in calibrating cutting force coefficients and calculating CWE, and the error caused by using linear cutting law, the tool orientations located in the boundary region between stable and unstable zones may lead to chatter. Moreover, the limiting cutting depth will change with the change of tool orientation. In order to improve machining stability, a machining stability factor is proposed as an index to select RTOs. Based on Eq. 24, the machining stability factor for the machining system is defined as:

$$
\left\{\begin{array}{l}\zeta(x,z,\alpha,\beta)=\dfrac{m\cos\gamma(\alpha,\beta)}{2}\min pos\left[\dfrac{R(E(\boldsymbol{\Phi}(x,z,\alpha,\beta,i\omega)))}{\left(1+\left(\dfrac{I(E(\boldsymbol{\Phi}(x,z,\alpha,\beta,i\omega)))}{R(E(\boldsymbol{\Phi}(x,z,\alpha,\beta,i\omega)))}\right)^2\right)}\right]\\ \omega=(1+\xi)\omega_n,\ \xi\in[\xi_{n,T,x},\xi_{n,T,y},\xi_{n,W}],\ \omega\in[\omega_{n,T,x},\omega_{n,T,y},\omega_{n,W}]\end{array}\right.
\tag{27}
$$

where $minpos$ represents to calculate the minimum positive value of the function, $E(\boldsymbol{\Phi}(x,z,\alpha,\beta,i\omega))$ represents to calculate the eigenvalue of the matrix $\boldsymbol{\Phi}(x,z,\alpha,\beta,i\omega)$. Equations 24 and 27 show that the tool orientation with a bigger value of machining stability factor would lead to a greater limiting cutting depth, and machining chatter is less likely to occur. The selection of RTOs at key CL points can be expressed as an optimization problem as follows:

$$
\begin{array}{l}Optimization\ Goal:\ \zeta(x,z,\alpha,\beta)\rightarrow\max\\ s.t.\quad chatter-free\ condition\ (Nyquist\ criterion)\end{array}
\tag{28}
$$

where $\zeta(\alpha,\beta)\rightarrow\max$ means to take the larger value that tends to the maximum, the optimization constraint condition of chatter-free is checked using Eq. 26 according to Nyquist criterion [27].

For calculating the stable region of tool orientation at the typical CL points, the sampling range and interval for the lead angle and tilt angle are selected. For a given tool orientation,

the CWEs, cutting force coefficient, and other parameters are calculated, and the stability of the tool orientation is judged according to the Nyquist stability criterion. After the machining stability of the tool orientations in the sampling range has been checked, the boundary between the stable region and the chatter region can be obtained. Meanwhile, the machining stability factors for the tool orientations are calculated. Then, the tool orientation located in the stable region and with a larger cutting stability factor is selected as the RTO of the typical CL point.

After the RTOs at crucial CL points are selected, spherical QI is used to interpolate smooth tool orientations at general areas. For the given two vectors $\boldsymbol{A}_1$ and $\boldsymbol{A}_n$, a formula for spherical QI from $\boldsymbol{A}_1$ to $\boldsymbol{A}_n$, with parameter i moving from 2 to $n-1$, can be obtained as [28]:

$$\boldsymbol{A}_i = \frac{\sin(\theta - \frac{i-1}{n-1}\theta)}{\sin\theta}\boldsymbol{A}_1 + \frac{\sin(\frac{i-1}{n-1}\theta)}{\sin\theta}\boldsymbol{A}_n, i \in [2, n-1] \tag{29}$$

where $\theta = \cos^{-1}(\boldsymbol{A}_1 \cdot \boldsymbol{A}_n)$, and $\boldsymbol{A}_i$ is the interpolated tool orientation. If $\boldsymbol{A}_1$ and $\boldsymbol{A}_n$ are close, a linear interpolation is used to avoid division by zero.

In the third step, the algorithms of checking chatter and adjusting tool orientation are used to verify and correct the generated tool orientations, respectively. If there is no chatter occurs for the CL data generated by the previous step, the tool orientations generated from Eq. 29 are used for five-axis CNC machining. If chatter appears, the chatter CL points are identified, assuming the chatter tool orientation is (α_i, β_i) at the ith chatter CL point. Next, the chatter tool orientation is adjusted to the chatter-free direction. The chatter-free tool orientation is determined so that the smallest tool orientation distance, $f_{min}(\alpha_i^c, \beta_i^c)$, is achieved between the chatter tool orientation (α_i, β_i) and its candidate chatter-free tool orientation (α_i^c, β_i^c). The tool orientation adjustment can be presented as a minimization problem as follows:

$$\begin{aligned} &\min \quad f(\alpha_i^c, \beta_i^c) = \left\{(\alpha_i^c - \alpha_i)^2 + (\beta_i^c - \beta_i)^2\right\} \\ &s.t. \quad chatter - free\ condition\ (Nyquist\ criterion) \end{aligned} \tag{30}$$

According to the Nyquist criterion [27], the constraint condition of chatter-free is checked by Eq. 26. The gradient method [29] is adopted to solve the optimization problem presented in Eq. 30. After a set of chatter-free tool orientations is determined at chatter CL points, these tool orientations are added to the RTOs list. The procedures of generating the tool orientations and checking the machining stability are carried out again until the tool orientations for all CL points are chatter-free. In this paper, the cutting depths are selected through simulation to ensure that chatter-free tool paths can be generated through tool orientation optimization. If the cutting depth is too large, cutting chatter may occur for all tool orientations, and then Eq. 30 has no solution. At this time, stable cutting can be ensured by reducing the cutting depth, adjusting the cutting speed, or increasing the rigidity of the cutting system.

The procedure of generating chatter-free tool orientations is shown in Fig. 3, it can be summarized as follows:

1. Select the typical CL points along the cutting path, get the stable tool orientation region by Eq. 26 based on Nyquist criterion, calculate machining stability factor by Eq. 27, select the tool orientation, and obtain the RTOs.
2. Interpolate smooth tool orientations at general areas from the RTOs by the QI algorithm as shown in Eq. 29.
3. Check machining stability at each CL point by Eq. 26 based on Nyquist criterion, if no chatter occurs, the tool orientations generated in the previous step are used for five-axis CNC machining.
4. If chatter occurs, the steepest descent method is used to solve (30) to determine the chatter-free tool orientations at the chattering CL points, and then add these tool orientations to the RTOs, go to step 2.

5 Simulations and experimental verification

The milling of the block workpiece (Fig. 4), the thin-walled part with curved surfaces (Fig. 9a), and the thin-walled blade (Fig. 17a) were carried out on a five-axis machining center JD GR200-A10SH with the maximum spindle speed of 28,000 rpm. The workpiece material is titanium alloy with a density of 4500 kg/m^3, Young's modulus of 104 GPa, and Poisson's ratio of 0.305. The 4-fluted ball-end mills with 8 mm diameter were used in the tests. An impact hammer Dytran Model 5800B, an accelerometer Dytran 3224A1, and the data acquisition system ECON-AVANT-8008 were used in the tests.

To identify the state of the machining process, the accelerometer was used to collect acceleration signals of the machining system, the sampling rate was set to 25600 Hz. The mobile roughness measuring instrument Masurf M300C was used to measure the surface roughness of blades. For each area, measurements were repeated three times and the average value was calculated. The occurrence of chatter is identified by checking the spectrum of the acceleration signals at frequencies close to the natural frequencies of the machining system but not coinciding with the tooth passing frequency (TPF) and its harmonics. Moreover, the chatter can be identified by the appearance of chatter marks on the machined surface.

5.1 Example 1 — milling of block workpiece

The FRFs of the tool were measured at three locations in x and y directions, as shown in Fig. 5. Due to the inability to attach the sensor to the tipping point of the tool, when measuring the dynamic parameters of the tool axis system, the

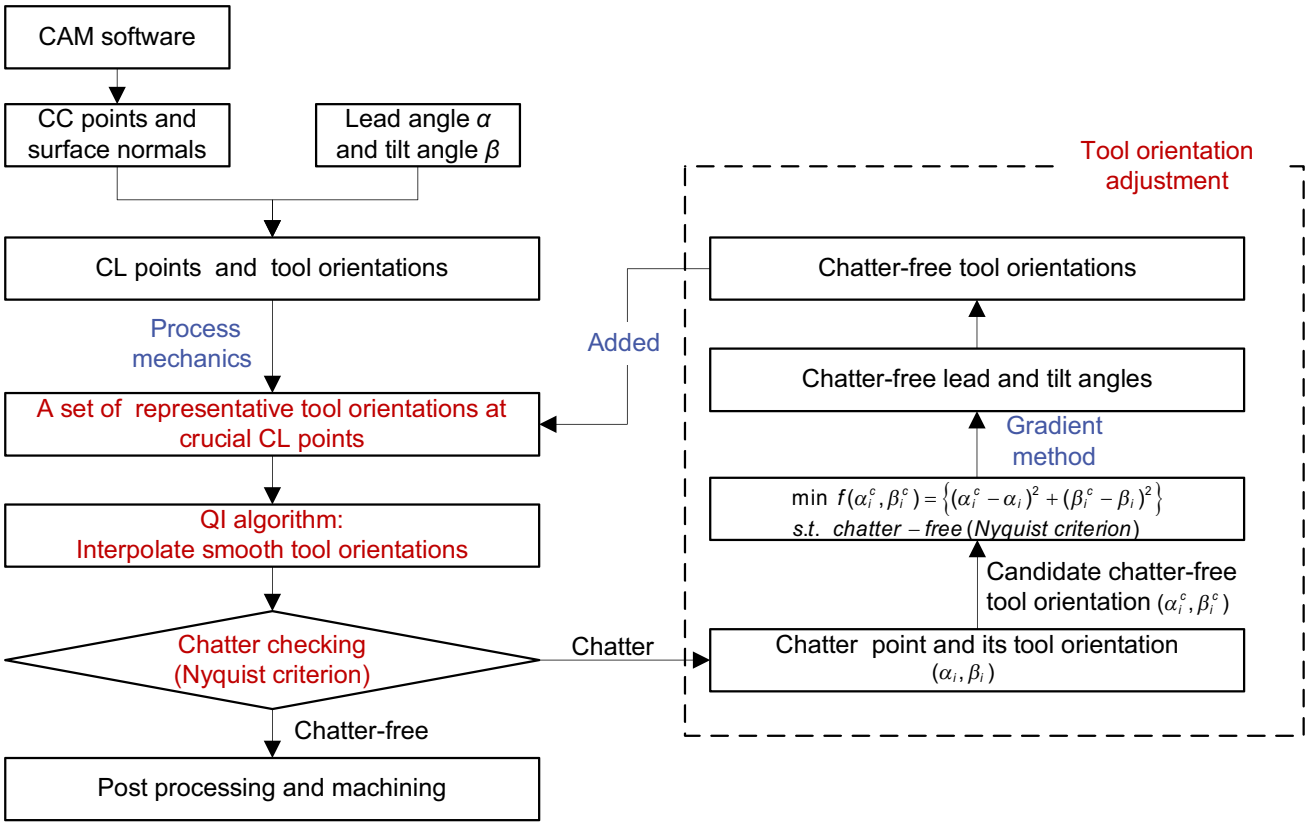

Fig. 3 The block diagram of the procedures of generating chatter-free and smooth tool path

Fig. 4 Tool path for Example 1 with the cutting depth of 0.6 mm

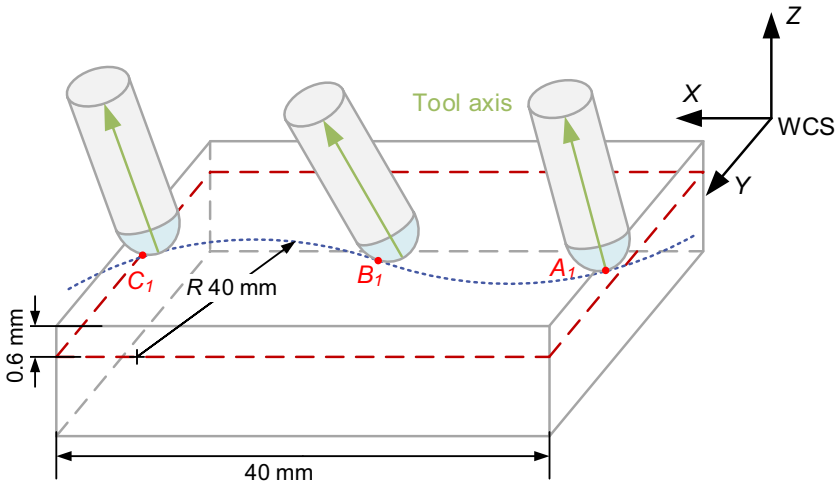

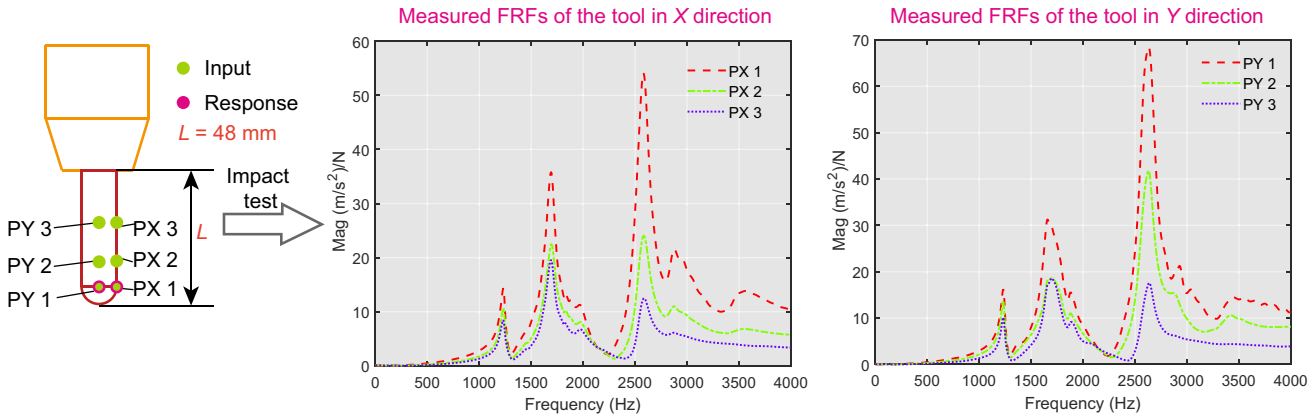

Fig. 5 Measurement points of impact tests and measured FRFs of tool

sensor was attached to the position located approximately 4 mm above the tipping point of the cutter. The measurement points PX1/PY1, PX2/PY2, and PX3/PY3 were located at 4, 15, and 30 mm away from the cutter tip. For the x-direction test, the accelerometer was fixed at PX1, while the tool was respectively excited at PX1, PX2, and PX3. For the y-direction test, the accelerometer was fixed at PY1, while the tool was excited at PY1, PY2, and PY3. The identified frequency, damping ratio and mode shapes of the tool are presented in Table 1.

The fitting model of the cutting force coefficient proposed in [26] is used to calculate the cutting force coefficient. The fitting model is written as:

$$K_x = W_0 + W_1 z + W_2 z^2 + W_3 z^3 + W_4 z^4 + W_5 n + W_6 n^2 + W_7 n^3, \quad (x = tc, rc, ac, te, re, ae) \tag{31}$$

where z is the position of the cutting element, that is, the distance from the cutting element to the tool tip along the axial direction, and the unit of z is mm; n is the spindle speed, and the unit of n is rpm. The values of W_0, W_1, W_2, W_3, W_4, W_5, W_6, and W_7 are shown in Table 2.

To determine the cutting depth used in the simulation, the method proposed in Section 3 is used to calculate limiting cutting depth. Meanwhile, to illustrate the advantage of the proposed method in Section 3, a comparison analysis was conducted between the proposed method and the method presented in reference [10] for calculating the limiting cutting depth. For the CL point A_1 and the tool orientation of $(\alpha, \beta) = (20°, 20°)$, the convergence process of calculating the absolute stability limiting cutting depth is depicted in Table 3 and Table 4. It shows that compared with the method presented in reference [10], the method proposed in Section 3 can quickly calculate the limiting cutting depth. Moreover, the method proposed in the reference [10] relies on the selected initial cutting depth and the increment of cutting depth Δa, the method proposed in this article does not have this shortcoming.

In this part, the tool is flexible and the workpiece is rigid, the dynamic parameters of the workpiece are set to 0 in the calculation process. The chatter-free tool orientations at each crucial CL point are obtained using Eq. 26 according to Nyquist criterion [27]. The predicted feasible tool orientations and calculated stability factor at location B_1 are shown in Fig. 6. According to Fig. 6, at location B_1, the inclination angle of $(\alpha, \beta) = (10°, 5°)$ is an unstable tool orientation, the inclination angles of $(\alpha, \beta) = (25°, 5°)$ and $(\alpha, \beta) = (25°, 20°)$ are the stable tool orientations but with different stability factors. Figure 6 shows that the stability factor for the tool orientation of $(\alpha, \beta) = (25°, 20°)$ is bigger than that for the tool orientation

Table 1 Identified modal parameters in x and y directions for the tool with the overhang of 48 mm

Direction	Mode	Frequency (Hz)	Damping ratio (%)	Mass normalized mode shape ($1/\sqrt{\text{kg}}$)
x	1	1233	1.335	[0.5621, 0.4608, 0.3764]
	2	1685	2.727	[1.3034, 0.8499, 0.7323]
	3	2575	1.816	[1.3761, 0.5993, 0.2961]
	4	2875	2.889	[0.3213, −0.0062, 0.0213]
y	1	1234	1.158	[0.6122, 0.4089, 0.4361]
	2	1682	4.456	[1.6495, 0.8225, 1.0711]
	3	2615	2.237	[1.7613, 1.0587, 0.4420]
	4	2954	1.284	[0.3943, −0.0015, 0.0002]

Table 2 The fitted polynomial coefficients of K_{tc}, K_{rc}, K_{ac}, K_{te}, K_{re}, K_{ae}

	K_{tc}	K_{rc}	K_{ac}	K_{te}	K_{re}	K_{ae}
W_0	2806.58	1645.38	−1361.96	−12.02	1.3	−2.91
W_1	−5234.37	−4189.23	3679.93	−14.5	−1.7	4.41
W_2	4254.6	4025.75	−3872.36	19.06	−7.9	−8.41
W_3	−1494.65	−1634.1	1710.31	−10.17	6.4	3.99
W_4	191.41	237.468	−267.88	1.87	−1.26	−0.54
W_5	0.67	0.46	0.29	0.018	2.87×10^{-3}	4.14×10^{-3}
W_6	-1.57×10^{-4}	-1.04×10^{-4}	-6.92×10^{-5}	-4.42×10^{-6}	-7.11×10^{-7}	-1.02×10^{-6}
W_7	1.22×10^{-8}	7.82×10^{-9}	5.32×10^{-9}	3.55×10^{-10}	5.73×10^{-11}	8.05×10^{-11}

of $(\alpha, \beta) = (25°, 5°)$, this means the machining process with $(\alpha, \beta) = (25°, 20°)$ is more stable than the machining process with $(\alpha, \beta) = (25°, 5°)$.

To verify the accuracy of the predictions, three tests were carried out and the tool orientations along the whole tool path were fixed at $(\alpha, \beta) = (10°, 5°)$, $(\alpha, \beta) = (25°, 5°)$ and $(\alpha, \beta) = (25°, 20°)$, respectively. The accelerometer was attached to the stator of the spindle to measure the acceleration signals. The machined surfaces, the measured surface roughness, the measured acceleration signals, and the spectral analysis of the acceleration signals are shown in Fig. 7. For spectral analysis, the signals within a period of time near the CL points A_1, B_1, and C_1 are selected for Fourier transform to determine the cutting status. In Fig. 7, $A_{1,Adj}$, $B_{1,Adj}$, and $C_{1,Adj}$ respectively represent a segment of acceleration signals in the adjacent areas of CL points A_1, B_1, and C_1.

As can be seen from Fig. 7, at the location B_1, the tool orientation of $(\alpha, \beta) = (10°, 5°)$ leads to the chatter at frequency 2945 Hz, and produces a rough finished surface, the chatter is caused by the fourth-order natural frequency of tool at 2875 Hz or 2954 Hz; the tool orientations of $(\alpha, \beta) = (25°, 5°)$ and $(\alpha, \beta) = (25°, 20°)$ diminish the chatter, the acceleration spectrum is dominated by the TPF (433 Hz) which is caused by forced vibrations. Moreover, compared with the tool orientation of $(\alpha, \beta) = (25°, 5°)$, the tool orientation of $(\alpha, \beta) = (25°, 20°)$ leads to the smaller amplitude of acceleration signal. The amplitude of the acceleration signal represents the vibration intensity of the machining system. In addition, the tool orientation of $(\alpha, \beta) = (25°, 5°)$ leads to chatter at locations A_1 and C_1, the chatter frequency (CF) is 2946 Hz which is caused by the fourth-order natural frequency of tool at 2875 Hz or 2954 Hz. The tool orientation of $(\alpha, \beta) = (25°, 20°)$ leads to chatter at location A_1 and the CF is 2964 Hz which is caused by the fourth-order natural frequency of the tool at 2875 Hz or 2954 Hz, but this tool orientation diminishes the chatter at location C_1. These results mean that compared with the tool orientation of $(\alpha, \beta) = (25°, 5°)$, the tool orientation of $(\alpha, \beta) = (25°, 20°)$ leads to a more stable machining process. The above experimental results are in accordance with the simulation results.

The experimental results show that the CF during the milling process is somewhat different from the measured natural frequency as shown in Table 1. This is because the contact between the tool and the workpiece during the machining process is equivalent to applying a support to the tool at the tip position, the rigidity and the natural frequency of the tool are improved.

The spectral analysis indicates that the tool orientation of $(\alpha, \beta) = (25°, 5°)$ and the tool orientation of $(\alpha, \beta) = (25°, 20°)$ can guarantee the milling stability at location B_1, however, these two tool orientations cannot guarantee the milling stability on the whole tool path. This is because the change of feed direction (F) along the curved tool path leads to the continuous change of CWE, which leads to the milling process being stable at location B_1 while it is unstable at location A_1. Hence, the tool orientations need to be replanned.

In order to demonstrate the proposed tool orientation optimization method, according to the predicted feasible tool orientations and calculated machining stability factors, the inclination angles of tool at locations A_1, B_1 and C_1 are set to $(\alpha, \beta) = (30°, 15°)$, $(\alpha, \beta) = (25°, 20°)$, $(\alpha, \beta) = (20°, 25°)$, respec-

Table 3 The convergence process of the absolute stability limiting cutting depth calculated by the proposed method (unit: mm)

Cutting depth in analysis	Calculated absolute stability limiting cutting depth	Difference	L	U	M
0.15	1.3	1.15	0.15	1.3	0.725
0.725	0.5515	0.1735	0.5515	0.725	0.63825
0.63825	0.5756	0.06265	0.5756	0.63825	0.6069
0.6069	0.591	0.0159	0.591	0.6069	0.599
0.599	0.596	0.003			

Table 4 The convergence process of the absolute stability limiting cutting depth calculated by the method presented in reference [10] (unit: mm)

Cutting depth in analysis	Calculated absolute stability limiting cutting depth	Difference
0.15	1.3	1.15
0.20	1.017	0.817
0.25	0.9019	0.6519
0.30	0.833	0.533
0.35	0.745	0.395
0.40	0.719	0.319
0.45	0.682	0.232
0.50	0.654	0.154
0.55	0.626	0.076
0.60	0.595	0.005

tively. The method proposed in Sect. 4 is used to generate the tool path. In the simulation calculation, the number of CL points is set to 20, and the number of CL points will be increased in the actual milling process. The tool orientations along the tool path are interpolated from the three initial RTOs using Eq. 29, and then, the machining stability is checked at each CL point. It can be found that chatter occurs at CL 7, and the inclination angle of tool orientation is $(\alpha, \beta) = (26.5734°, 18.4735°)$. The gradient method is used to solve the minimization problem as presented in Eq. 30, the initial candidate chatter-free tool orientation is selected as $(\alpha, \beta) = (28°, 19°)$, and the step-size is set as 0.25. After calculation, the chatter-free tool orientation at CL 7 is set to $(\alpha, \beta) = (27.2867°, 18.7368°)$, then, this tool orientation is added to the RTOs. The adjusted tool orientations are generated using Eq. 29 through the new RTOs. There is no chatter that occurs after the first adjustment, the generated tool orientations are used for five-axis CNC machining. The process for generating chatter-free and smooth tool orientations for milling of block workpiece is shown in Fig. 8a.

The machined surface, measured acceleration signal and the results of spectral analysis for the test with the optimized tool orientations are displayed in Fig. 8. The acceleration signal spectrum is dominated by the TPF of 433 Hz which is caused by forced vibration. Compared with the original tool orientations (Fig. 7), the optimized tool orientations (Fig. 8a) can ensure the stable machining along the whole tool path and obtain a smooth machined surface.

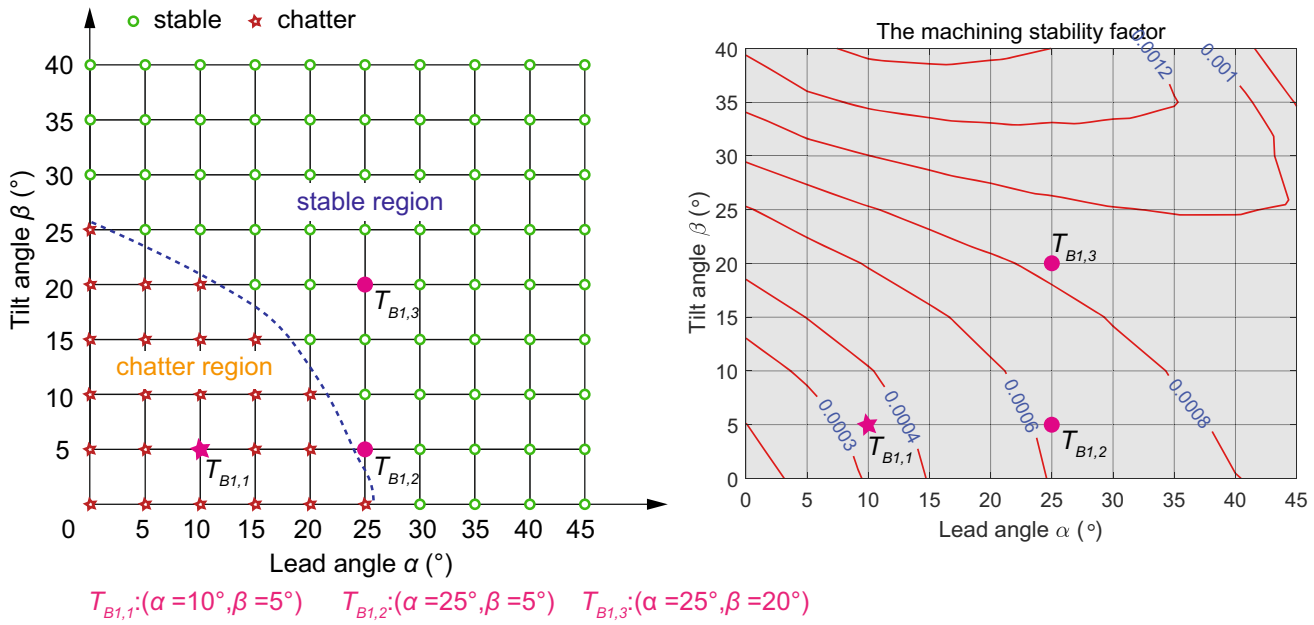

Fig. 6 The predicted feasible tool orientations and the changing trend of machining stability factor with the changes of tool orientation for location B_1

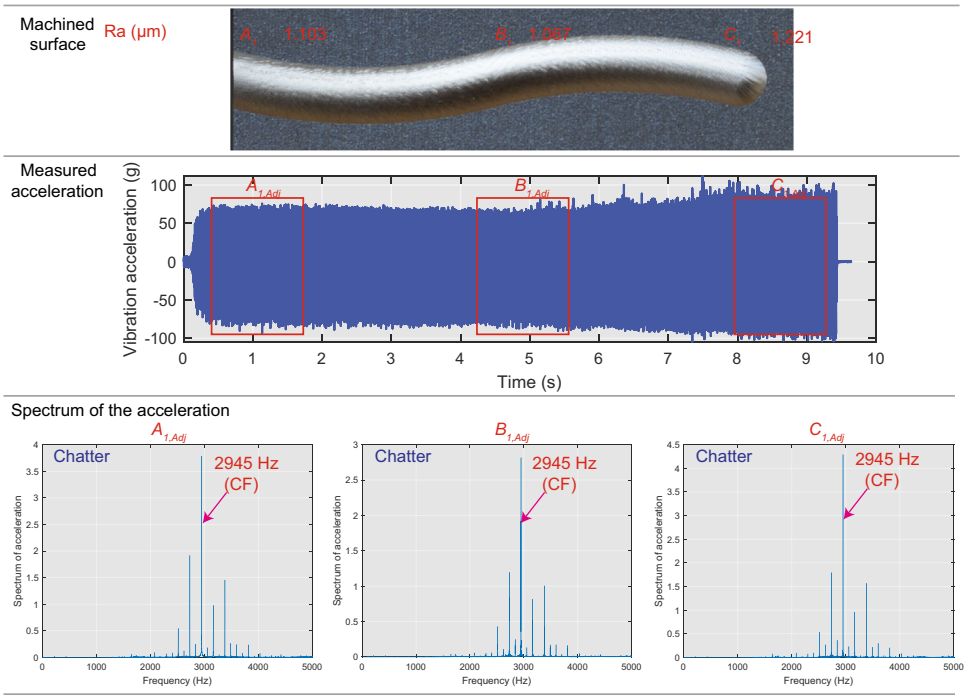

(a)

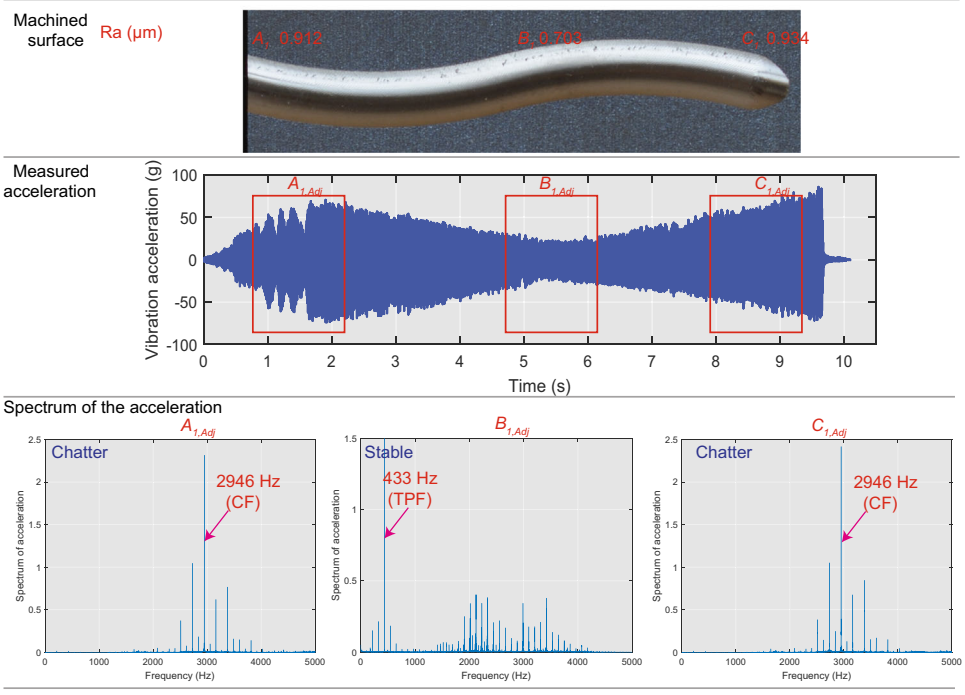

(b)

Fig. 7 Machined surfaces, measured acceleration signals and spectrum of the acceleration signals for milling of block workpiece with unoptimized tool orientations: **a** $\alpha = 10°$, $\beta = 5°$; **b** $\alpha = 25°$, $\beta = 5°$; **c** $\alpha = 25°$, $\beta = 20°$

Fig. 7 continued

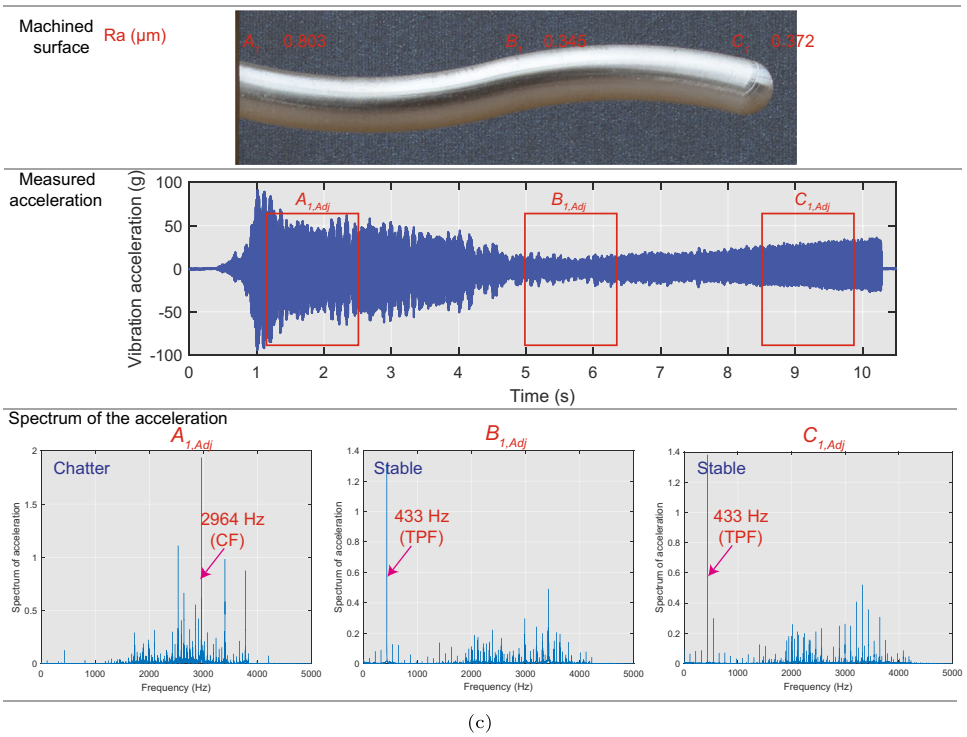

(c)

Fig. 8 **a** Generation of chatter-free and smooth tool orientations for milling of block workpiece; **b** machined surface, measured acceleration signal and spectrum of the acceleration signal for milling of block workpiece with optimized tool orientations

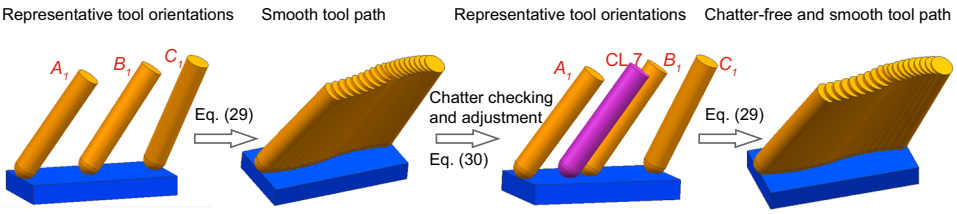

The lead and tilt angles of representative tool orientations

A_1 30°, 15° B_1 25°, 20° C_1 20°, 25°

Generating smooth tool orientations at CL points using Eq.(29) and checking the machining stability using Nyquist criterion

① 30°, 15° ② 29.4°, 15.6° ③ 28.8°, 16.2° ④ 28.2°, 16.8° ⑤ 27.7°, 17.4° ⑥ 27.1°, 17.9° ⑦ 26.5°, 18.4° (chatter)
⑧ 26.0°, 18.9° ⑨ 25.5°, 19.5° ⑩ 25°, 20° ⑪ 23.3°, 21.2° ⑫ 22.6°, 21.3° ⑬ 22.1°, 21.4° ⑭ 21.5°, 21.7°
⑮ 21.1°, 22.0° ⑯ 20.7°, 22.5° ⑰ 20.4°, 22.9° ⑱ 20.2°, 23.6° ⑲ 20.1°, 24.3° ⑳ 20°, 25°

Adjusting the chatter tool orientation of CL 7 to chatter-free tool orientation using Eq. (30)

Selecting the lead angle of 28° and tilt angle of 19° as the initial chtter-free tool orientation

Iterations	(α_i^c, β_i^c)	Step-size	$\nabla f(\alpha_i^c, \beta_i^c)$	$f(\alpha_i^c, \beta_i^c)$	State
0	(28°, 19°)	0.25	(2.8532, 1.0530)	2.3124	Stable
1	(27.2867°, 18.7368°)	0.25	(1.4266, 0.5265)	0.5781	Stable
2	(26.9301°, 18.6051°)	0.25	(0.7133, 0.2632)	0.1445	Chatter
3	(26.7517°, 18.5393°)	0.25	0.3567, 0.1316)	0.0361	Chatter

Setting the tool orientation of CL 7 as (27.2867°, 18.7368°)

Adding the chatter-free tool orientation of CL 7 to the representative tool orientations

A_1 30°, 15° CL 7 27.2867°, 18.7368° B_1 25°, 20° C_1 20°, 25°

The chatter-free and smooth tool orientation at each CL point

① 30°, 15° ② 29.5°, 15.6° ③ 29.1°, 16.3° ④ 28.6°, 16.9° ⑤ 28.2°, 17.5° ⑥ 27.7°, 18.1° ⑦ 27.3°, 18.7°
⑧ 26.5°, 19.2° ⑨ 25.7°, 19.6° ⑩ 25°, 20° ⑪ 23.3°, 21.2° ⑫ 22.6°, 21.3° ⑬ 22.1°, 21.4° ⑭ 21.5°, 21.7°
⑮ 21.1°, 22.0° ⑯ 20.7°, 22.5° ⑰ 20.4°, 22.9° ⑱ 20.2°, 23.6° ⑲ 20.1°, 24.3° ⑳ 20°, 25°

(a)

Fig. 8 continued

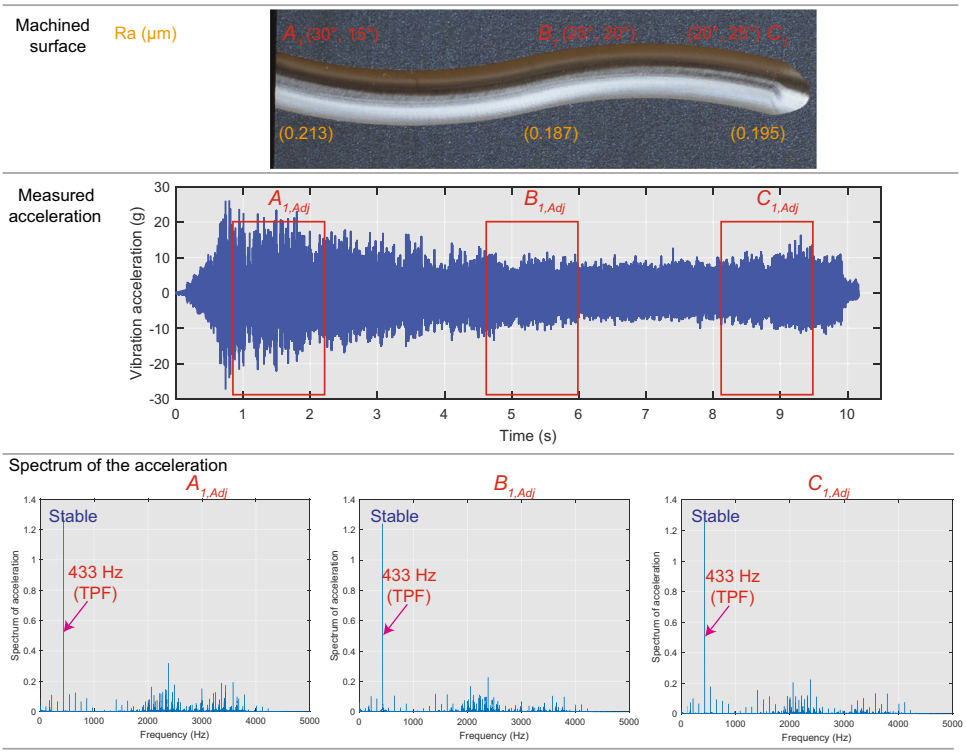

(b)

For the milling of the rectangular workpiece, 20 CL points are discretized along the tool path during simulation calculation, the ranges of lead and tilt angles are respectively set as $\alpha \in [0, 45°]$ and $\beta \in [0, 40°]$, and the sampling interval is set to $1°$. For the method presented in the reference [17–19], it is necessary to calculate the feasible tool orientation domain of 20 CL points, the number of calculations is $45 * 40 * 20$. For the algorithm proposed in this article, only 3 CL points need to be calculated, then the machining stability of 17 CL points is checked, and then an iterative calculation which contains 4 steps is performed to obtain the stable tool orientation, then the machining stability of 16 CL points are checked. The number of calculations is about $45 * 40 * 3 + 17 + 4 + 16$. From the above analysis, it can be seen that the proposed algorithm can improve computational efficiency.

5.2 Example 2 — milling of thin-walled part with curved surfaces

In this part, the milling of the curved thin-walled part (Fig. 9a) is used to validate the proposed tool orientation optimization algorithm. The overhang of tool was set at 50 mm, the depth of cut was fixed at 0.3 mm, the spindle speed was set at 7000 rpm, and the feed rate was set at 260 mm/min. The ranges of lead and tilt angles are respectively set as $\alpha \in [0, 45°]$ and $\beta \in [0, 40°]$, and the sampling interval is set to $1°$ for both lead and tilt angles.

The modal shapes of the thin-walled part are calculated by the method proposed in [30], the meshed model of the workpiece is shown in Fig. 9b, the calculated first three orders of modal shapes are shown in Fig. 9c. The damping ratio should be extracted from the impact test. For the impact test performed on the thin-walled part, the positions of the response and excitation points are shown in Fig. 10a. The accelerometer was fixed at point 3, while the thin-walled part was respectively excited at six points using an impact hammer. The identified natural frequency and damping ratio of the initial thin-walled part is presented in Table 5. For the tool with the overhang of 50 mm, the FRFs of the tool were measured at three locations in x and y directions, as shown in Fig. 10b. The measurement points PX1/PY1, PX2/PY2 and PX3/PY3 were located at 4, 15 and 30 mm away from the tool tip. The identified frequency, damping ratio, and mode shapes of the tool are presented in Table 6.

For the machining along $curve\ 32.5$, the machining system will change from flexible workpiece to flexible tool, and then to flexible workpiece. The machining along $curve\ 32.5$ is selected to verify the effectiveness of the proposed method, and the CL points A_2, B_2, and C_2 are selected as the typical

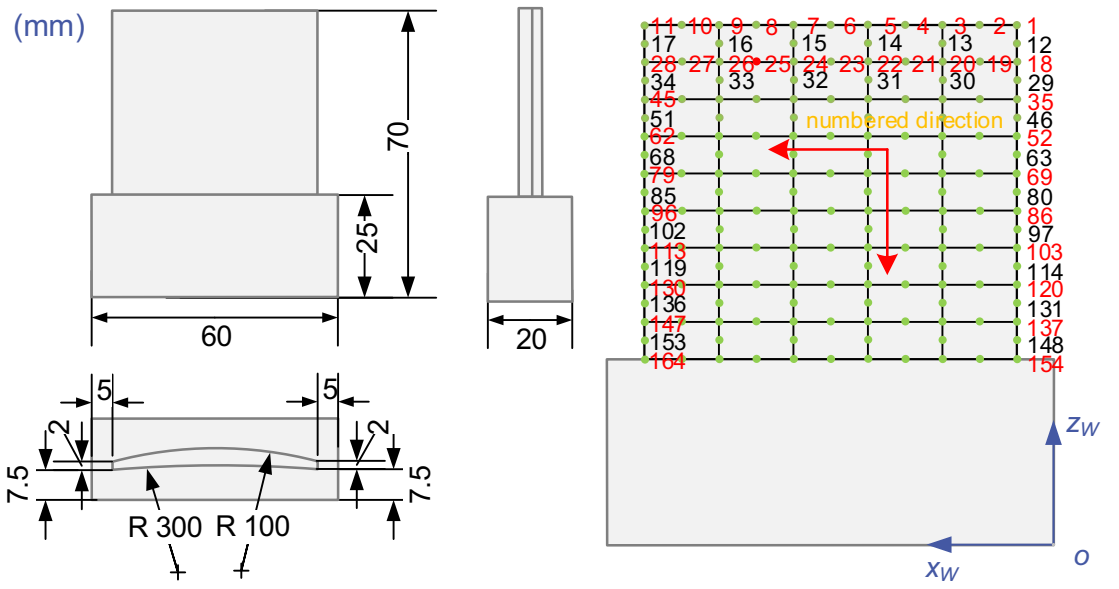

(a) (b)

Partial data of modal shape matrix

		Node 1	Node 2	Node 3	Node 4	Node 5	Node 6	Node 7	Node 8	Node 9	Node 10	Node 11
		1	2	3	4	5	6	7	8	9	10	11
Mode 1	1	-10.4225	-10.4165	-10.4051	-10.3912	-10.3795	-10.3724	-10.3713	-10.3762	-10.3855	-10.3954	-10.4018
Mode 2	2	16.7190	13.4213	10.0859	6.7348	3.3942	0.0769	-3.2139	-6.4748	-9.6931	-12.8433	-15.9045
Mode 3	3	-2.8455	-5.8402	-8.4459	-10.4125	-11.6359	-12.0160	-11.5790	-10.3341	-8.4107	-5.9395	-3.1635

Plotting modal shapes

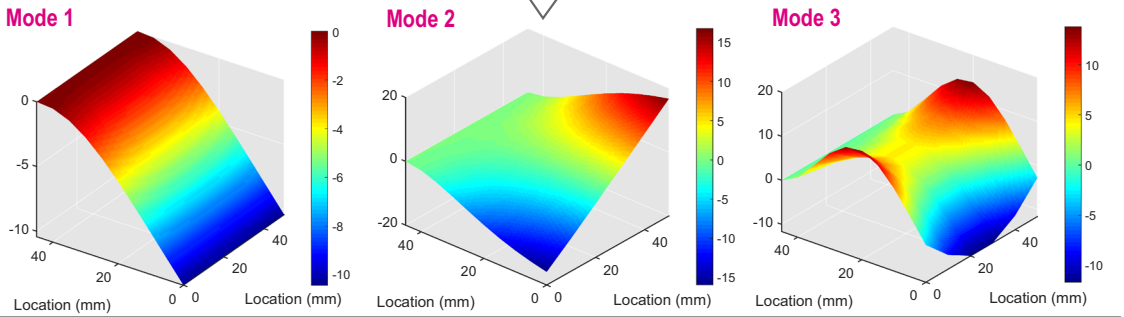

(c)

Fig. 9 **a** Dimension parameters of thin-walled part; and **b** meshing of thin-walled part and numbering of nodes; and **c** first three orders of modal shapes of thin-walled part

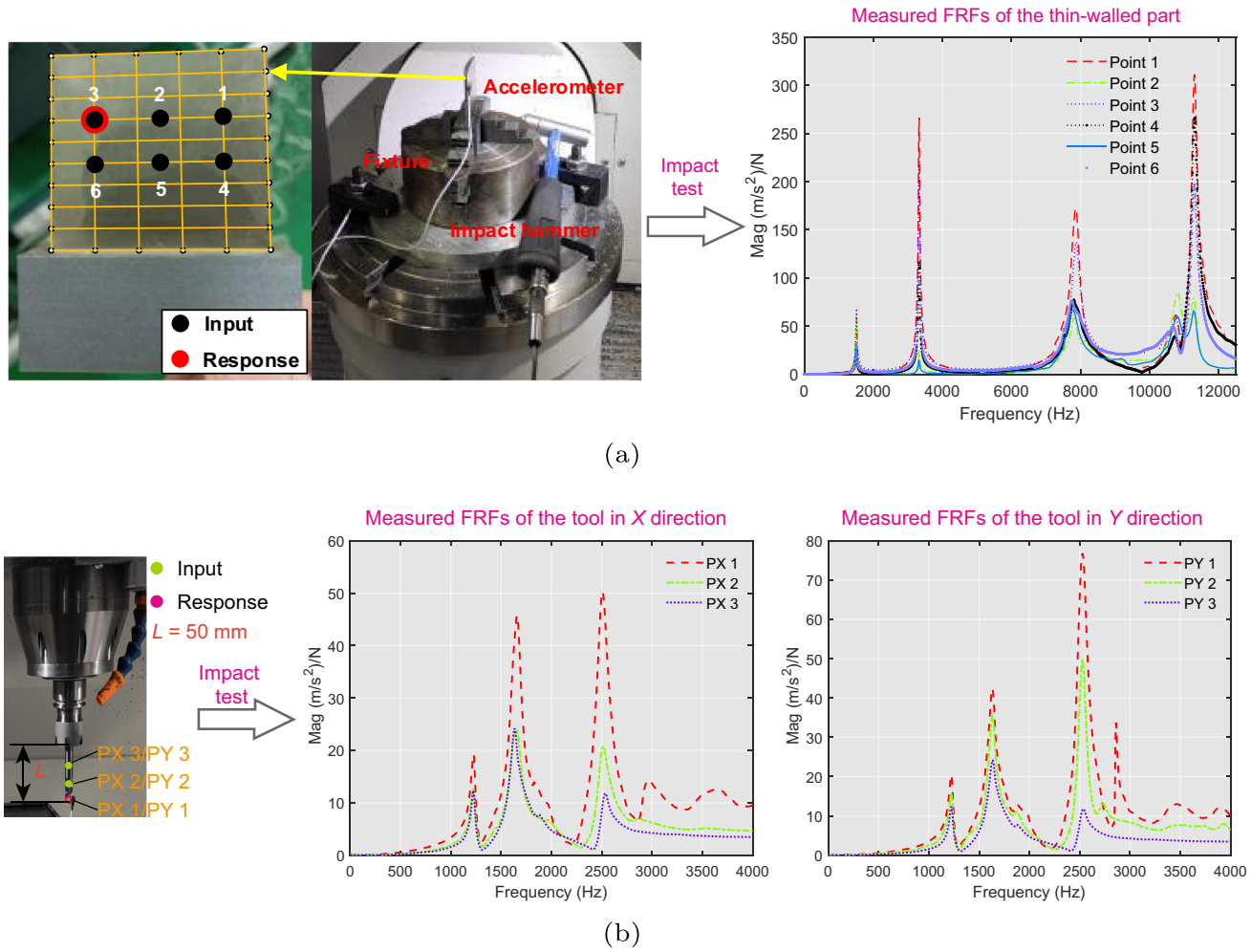

Fig. 10 Measurement points of impact tests and measured FRFs: **a** thin-walled part; and **b** tool

locations. At the locations A_2 and C_2, the dominant vibration mode is the second-order mode of the workpiece; at the location B_2, the tool is flexible while the workpiece is relatively rigid.

The relatively flexible body of the machining system will change during the milling of cantilever-shaped thin-walled parts. The dominant vibration mode of the machining system is determined by the limiting cutting depth, the mode with the lower limiting cutting depth is the dominant vibration mode. The workpiece is divided into three regions, the region where the dominant vibration mode is the first-order mode of the workpiece, the region where the dominant vibration mode is the second-order mode of the workpiece, the region where the tool is flexible, as shown in Fig. 11. The material removal will cause a change in workpiece dynamics in the milling process. The dynamic parameters of the thin-walled part during the milling process are calculated by the method proposed in the paper [30]. In order to calculate the dynamics of the workpiece in process, according to the cutting depth of 0.3 mm, the workpiece near the cutting area is meshed into elements with length of 3 mm along the z direction, as shown in Fig. 12. The process of obtaining stiffness and mass matrices of the workpiece in the process is shown in Fig. 12, then the workpiece dynamics can be calculated by the matrices. The calculated first three orders of frequency for different machining steps are shown in Table 7, and the calculated first three orders of modal shape along tool path for different machining steps are shown in Fig. 13. Step 1 to Step 5 respectively represents the workpiece has been machined along the tool path with the distance of 10 mm, 20 mm, 30 mm, 40 mm, and 50 mm. To improve the calculation accuracy, the dynam-

Table 5 Identified modal parameters for the initial curved thin-walled part

Mode	Frequency (Hz)	Damping ratio (%)
1	1575	1.227
2	3262	0.571
3	8293	1.203

Table 6 Identified modal parameters in x and y directions for the tool with the overhang of 50 mm

Direction	Mode	Frequency (Hz)	Damping ratio (%)	Mass normalized mode shape ($1/\sqrt{\text{kg}}$)
x	1	1225	1.599	[0.6682, 0.3868, 0.2872]
	2	1656	2.692	[1.4869, 0.7949, 0.6884]
	3	2511	1.800	[1.2593, 0.4949, 0.2327]
	4	2918	0.112	[0.3445, −0.0073, 0.0246]
y	1	1226	1.465	[0.7728, 0.7245, 0.4800]
	2	1627	2.912	[1.5063, 1.3509, 0.8882]
	3	2522	1.377	[1.4754, 0.9022, 0.2002]
	4	2851	0.119	[0.4147, −0.0021, −0.0003]

ics of the workpiece in the process as shown in Table 7 and Fig. 13 are used for simulations.

The predicted feasible tool orientations and calculated machining stability factors at the locations A_2 and C_2 are shown in Fig. 14. Moreover, in order to illustrate the necessity of considering both the flexible workpiece and tool during the milling of thin-walled parts, the model only considers the flexible workpiece and the model considers both flexible workpiece and tool respectively used to calculate the feasible tool orientations and machining stability factors at location B_2. The feasible tool orientations and machining stability factors calculated by the model only considering flexible workpiece are shown in Fig. 15a, the results calculated by the model considering both flexible workpiece and tool are shown in Fig. 15b.

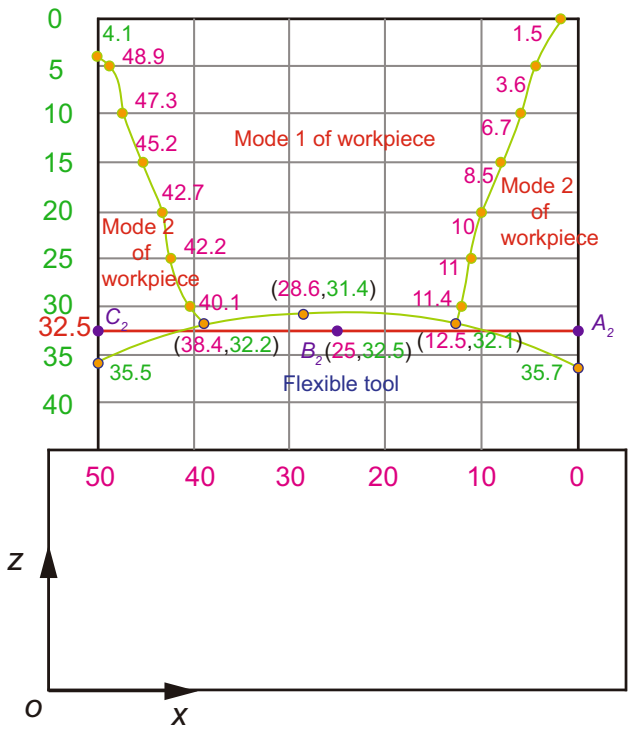

Fig. 11 Regions of thin-walled part which partitioned by dominant vibration modes of machining system

At location B_2, Fig. 15a shows that the inclination angle of $(\alpha, \beta) = (10°, 15°)$ is a stable tool orientation; however, Fig. 15b shows that this inclination angle is an unstable tool orientation, and the inclination angle of $(\alpha, \beta) = (20°, 20°)$ is a stable tool orientation. Since the tool is more flexible than the workpiece at location B, and the result presented in Fig. 15a only considers flexible workpiece, hence, the result presented in Fig. 15b should be used to select chatter-free tool orientations. To verify the simulation results, two tests along $curve$ 32.5 were carried out, and the tool orientations were fixed at $(\alpha, \beta) = (10°, 15°)$ and $(\alpha, \beta) = (20°, 20°)$, respectively. The vibration signals of the thin-walled part were obtained by the accelerometer attached to the free-end of workpiece.

The machined workpiece surfaces, the measured acceleration signals and the results of spectral analysis are shown in Fig. 16a. In the figure, $A_{2,Adj}$, $B_{2,Adj}$, and $C_{2,Adj}$ respectively represents a segment of acceleration signals in the adjacent areas of CL points A_2, B_2, and C_2. The tool orientation of $(\alpha, \beta) = (10°, 15°)$ leads to chatter along the whole tool path. The spectrums of acceleration signal are dominated by different vibration modes along the tool path. At location A_2, the chatter frequencies are 1330 Hz and 3267 Hz, the frequency of 1330 Hz is the chatter frequency of tool (CFT) which is caused by mode 1 of tool, the frequency of 3267 Hz is the chatter frequency of workpiece (CFW) which is caused by mode 2 of workpiece. Moreover, since the value of the spectrum of CFW is greater than that of CFT, the mode 2 of workpiece is the dominant vibration mode. At location B_2, the chatter frequencies are 1330 Hz and 3262 Hz which are respectively caused by mode 1 of tool and mode 2 of workpiece. The mode 1 of tool is the dominant vibration mode. At location C_2, the chatter frequencies are 1330 Hz and 3256 Hz which are respectively caused by mode 1 of tool and mode 2 of workpiece. The mode 2 of the workpiece is the dominant vibration mode. The changes of the natural frequency of workpiece are caused by the material removal during milling process. For the tool orientation of $(\alpha, \beta) = (20°, 20°)$, the changes of CWE and workpiece dynam-

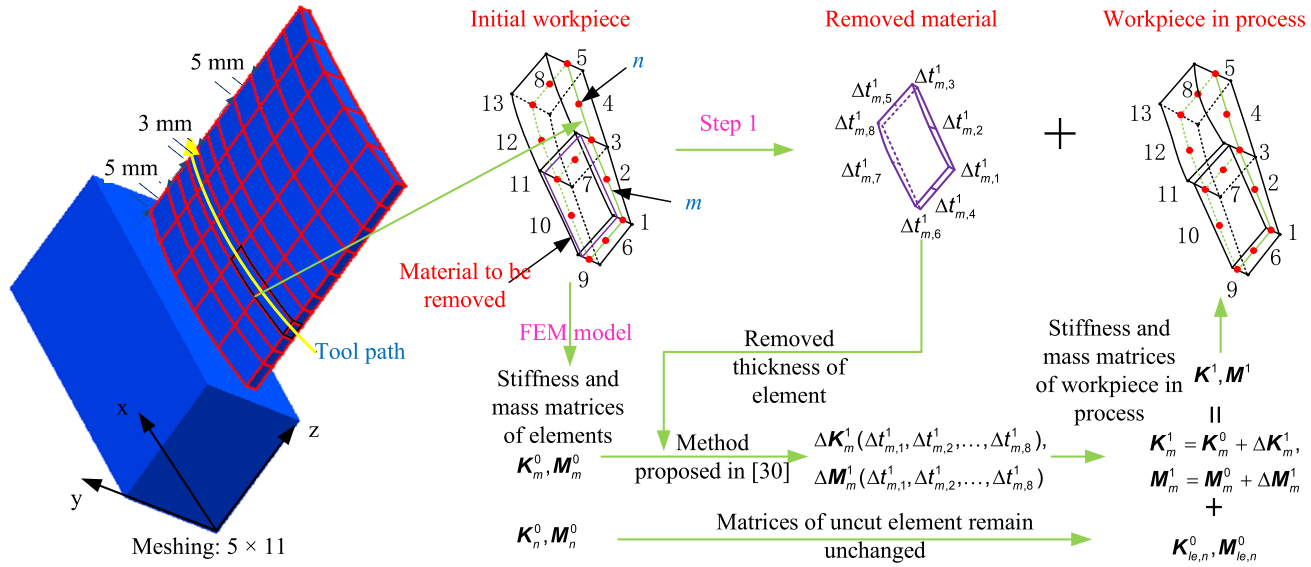

Fig. 12 Process of obtaining stiffness and mass matrices of workpiece in process

ics along the tool path lead to the milling process being stable at location B_2, while it is unstable at locations A_2 and C_2. At location A_2, the vibration frequencies are 1400 Hz and 3269 Hz, the frequency of 1400 Hz is the harmonic of TPF, and the frequency of 3269 Hz is the CFW which is caused by mode 2 of the workpiece. At location B_2, the vibration frequency is 1400 Hz which is the harmonic of TPF. At location C_2, the vibration frequencies are 1400 Hz and 3259 Hz, the frequency of 1400 Hz is the harmonic of TPF, and the frequency of 3259 Hz is the CFW which is caused by mode 2 of the workpiece. At CL points A_2 and B_2, the simulation results are consistent with the test results. However, at CL point C_2, there is some difference between simulation and test. Figure 14 shows that the tool orientation of $(\alpha, \beta) = (20°, 20°)$ is located in the machining stability region, but chatter occurs during milling process as shown in Fig. 16a. This is because there are calculation errors in the dynamic parameters of the thin-walled part, CWE, etc. As a result, there is a certain error in the calculated stable tool orientation region. As the tool orientation of $(\alpha, \beta) = (20°, 20°)$ is located at the boundary region between the stable region and chatter region as shown in Fig. 14b. The predicted stable tool orientation causes chatter during machining. Therefore, the tool orientation farther from the boundary should be selected.

Table 7 First three orders of frequency (Hz) of thin-walled part for different machining steps

	Step 1	Step 2	Step 3	Step 4	Step 5
Mode 1	1570	1567	1562	1557	1554
Mode 2	3260	3253	3245	3238	3233
Mode 3	8292	8288	8286	8282	8280

The results presented in Fig. 16a are consistent with the simulation results that at location B_2, the angle of $(\alpha, \beta) = (10°, 15°)$ is an unstable tool orientation while the angle of $(\alpha, \beta) = (20°, 20°)$ is a stable tool orientation. And, at location B_2, the mode of tool is the dominant vibration mode, while at locations A_2 and C_2, the mode 2 of the workpiece is the dominant vibration mode. The simulation and test results indicate that it is important to consider both the flexible workpiece and flexible tool during milling of thin-walled parts.

To generate chatter-free tool orientations along tool path, according to the predicted feasible tool orientations and calculated machining stability factors, the lead and tilt angles of tool at locations A_2, B_2 and C_2 are set as $(\alpha, \beta) = (30°, 20°)$, $(\alpha, \beta) = (20°, 20°)$, $(\alpha, \beta) = (30°, 20°)$, respectively. After the tool orientations along the tool path are interpolated from the three initial RTOs, the machining stability is checked at each CL point. In this case, there is no chatter occurs for the tool orientations generated by the second step of the proposed method, it does not need iterative calculations. The generated chatter-free tool orientations along the tool path, the machined workpiece surface, the measured acceleration signals, and the results of spectral analysis of the signal are shown in Fig. 16b.

Figure 16 shows that compared with the tool orientations of $(\alpha, \beta) = (10°, 15°)$ and $(\alpha, \beta) = (20°, 20°)$, the optimized tool orientations lead the amplitude of the acceleration signal to decrease significantly. Moreover, for the milling with optimized tool orientations, the spectrum of the acceleration signal is dominated by TPF (466 Hz) and its harmonic (1400 Hz) which means the machining process is stable along the whole tool path. Both the result of the frequency spectrum of the acceleration response and the quality of the machined surface show that the optimized tool orientations can sup-

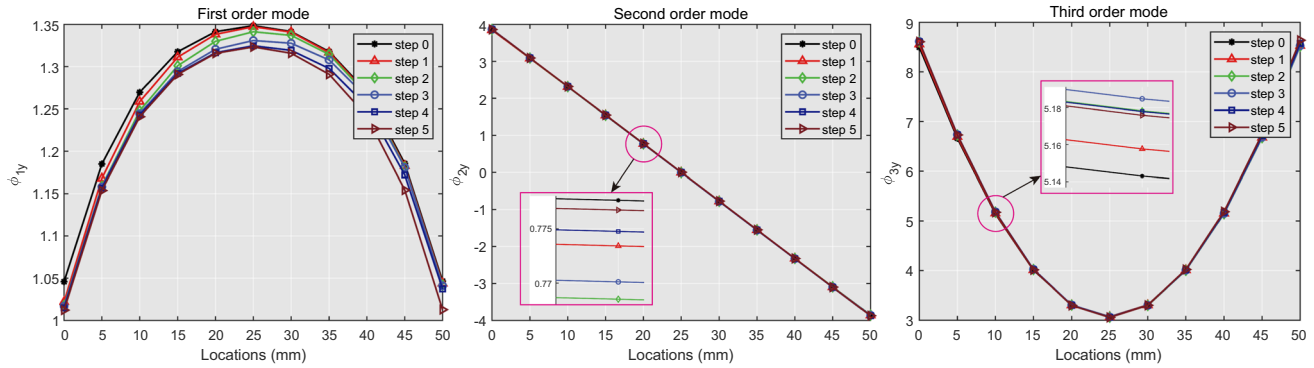

Fig. 13 First three orders of the modal shape of the thin-walled part along tool path for different machining steps

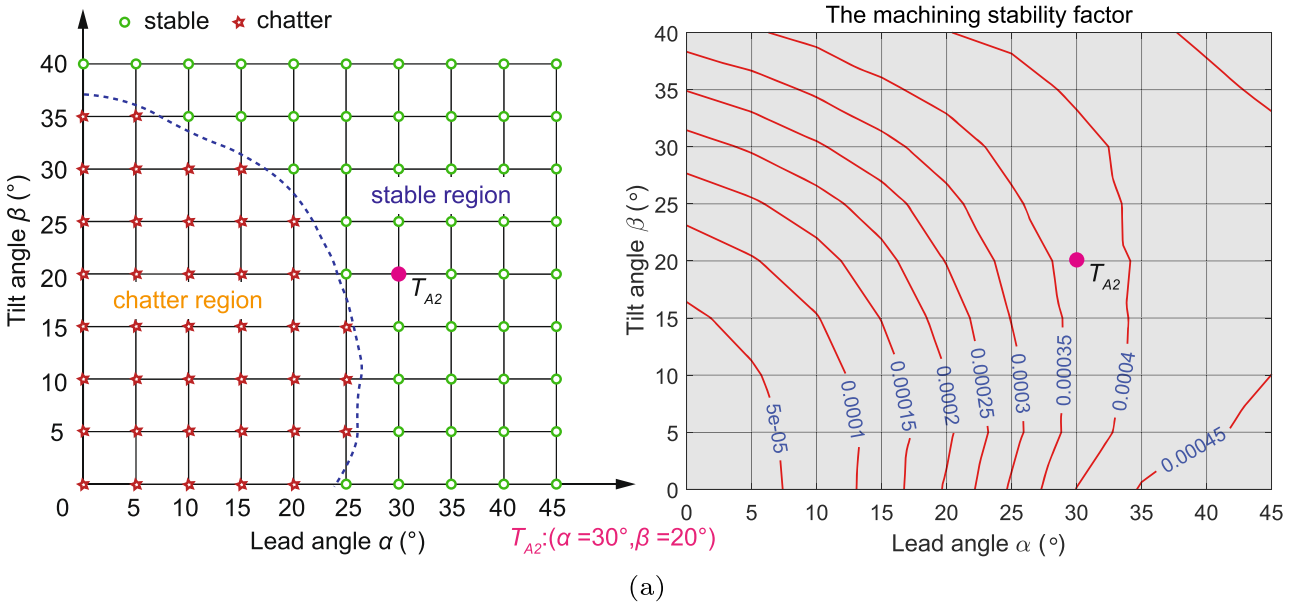

(a)

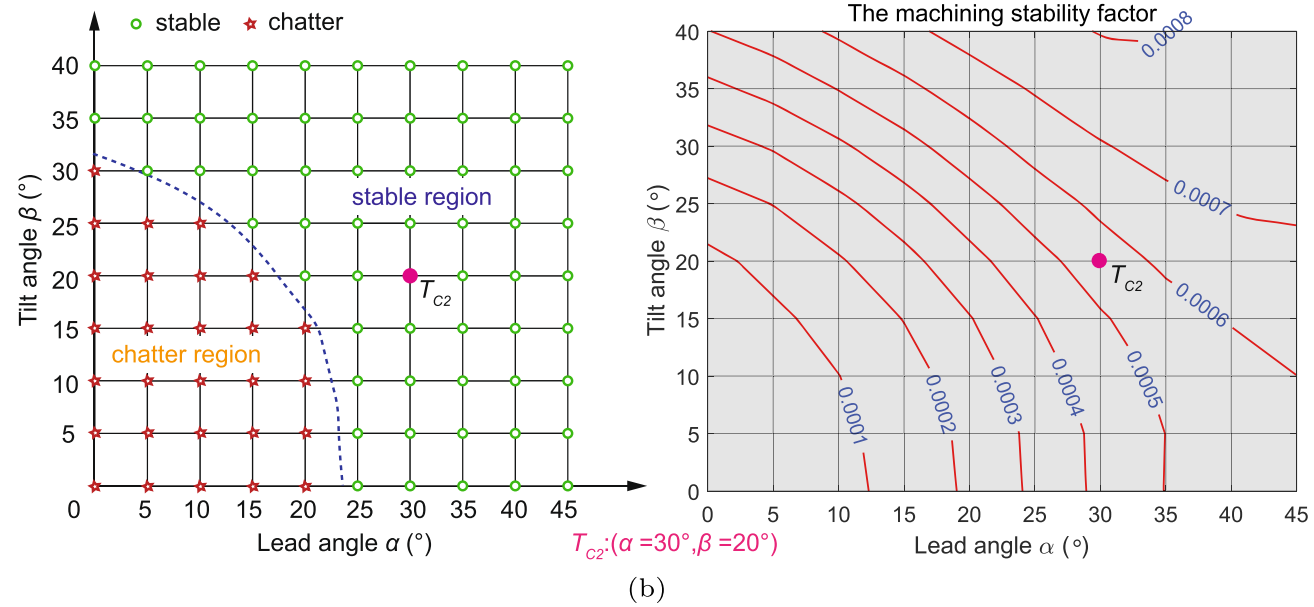

(b)

Fig. 14 The predicted feasible tool orientations and calculated machining stability factors at the point on *curve* 32.5: **a** A_2; and **b** C_2

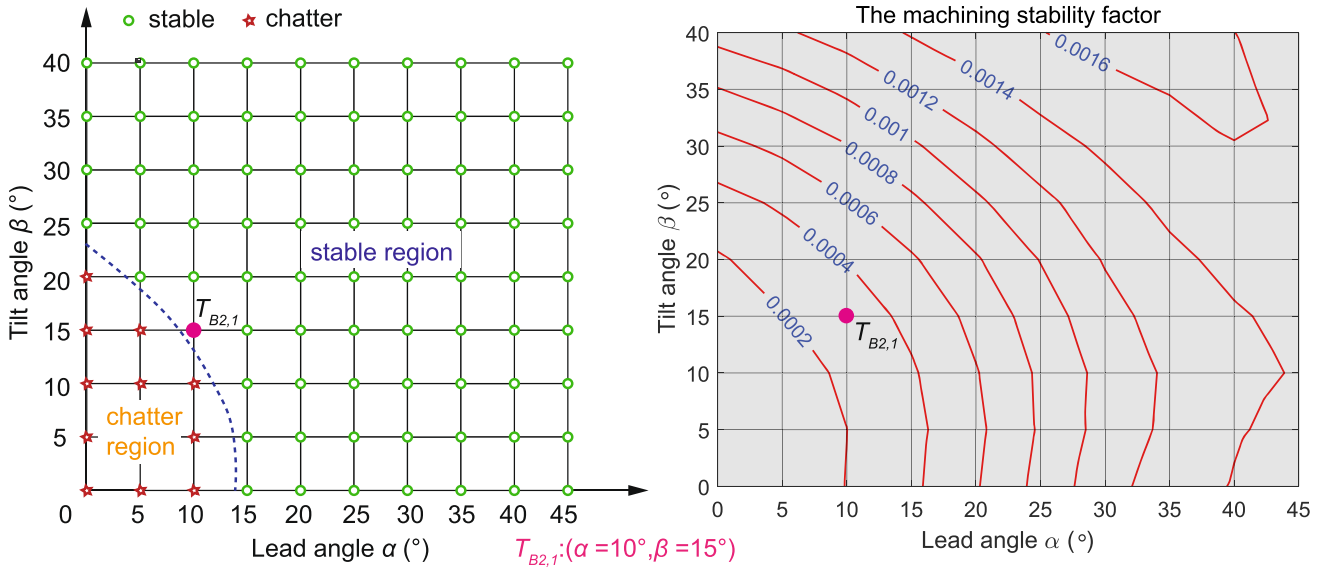

(a)

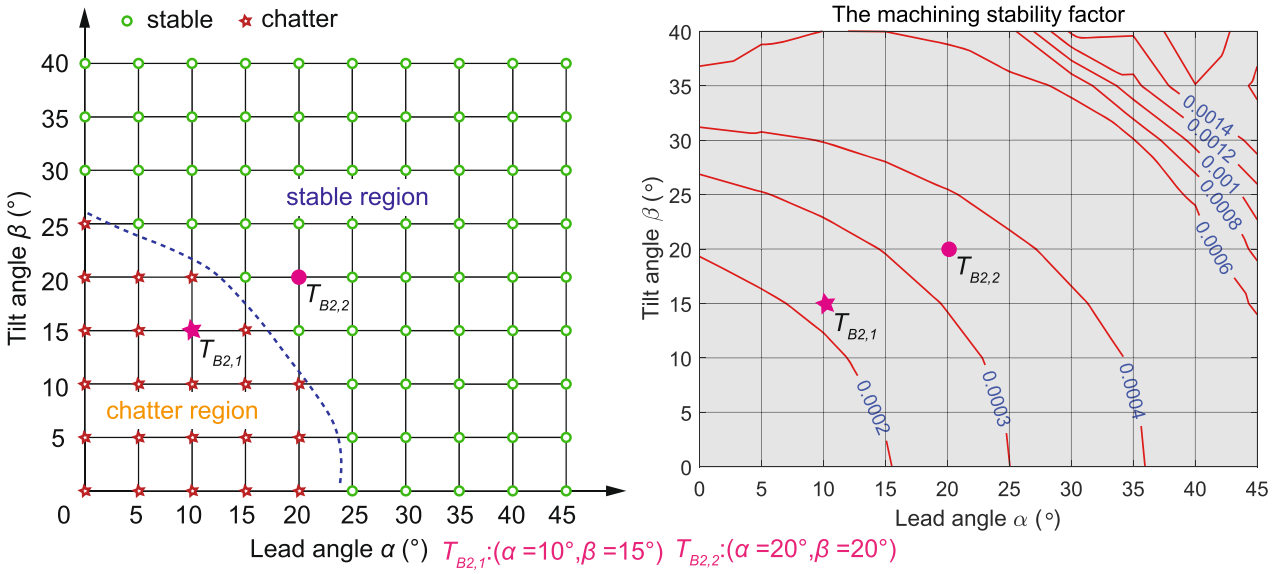

(b)

Fig. 15 The predicted feasible tool orientations and calculated machining stability factors at the location B_2 on *curve* 32.5: **a** calculated by the model only considers flexible workpiece; and **b** calculated by the model considers both flexible workpiece and tool

press chatter and improve the machining stability in five-axis ball-end milling of curved thin-walled part.

5.3 Example 3 — milling of thin-walled blade

In this section, the proposed method is used for the milling of thin-walled blade, as shown in Fig. 17a. The lengths of the inlet and exhaust sides are both 45.0 mm. The thicknesses at the thinnest and thickest positions of the blade are 0.83 mm and 2.45 mm respectively, which is a twisted structure. The points 1, 2, 3, 4, 5, 6, 7, and 8 are selected as the typical CL points, as shown in Fig. 17a.

The calculated feasible tool orientation regions and machining stability factors at CL points 2 and 4 are shown in Fig. 17b and c. According to the calculated results, the tool orientations at the CL points 2, 3, 4, 6, 7, and 8 are set to (35°, 30°), the tool orientations at CL points 1 and 5 are set to

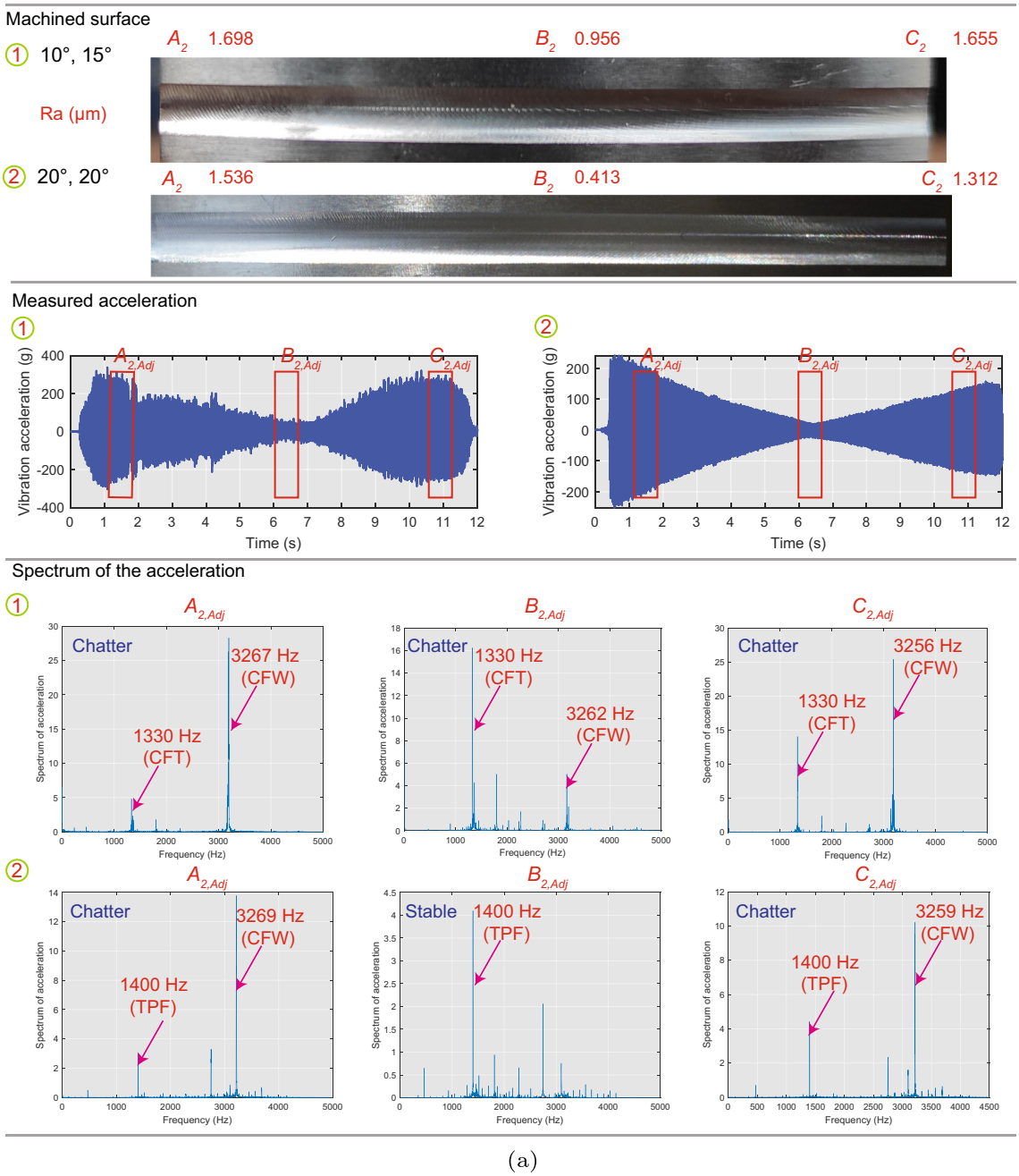

Fig. 16 Machined surface, measured acceleration signals, and spectrum of the acceleration signals for milling of thin-walled parts with: **a** unoptimized tool orientations; **b** chatter-free and smooth tool orientations generated by the proposed method

(45°, 30°). Then, the proposed method is used to generate the optimized and smooth tool orientations along the tool path, as shown in Fig. 17d

The milling of thin-walled blade was carried out on the five-axis machining center JD GR200-A10SH. The blank was a rectangular workpiece, its size was 50 mm×20 mm× 70 mm, and its material was titanium alloy TC4.

The blades were cut according to the rough machining, semi-finishing machining, and finishing machining process. During rough machining, the peripheral milling method was used to remove most of the allowance; the spiral circumferential milling method was used in semi-finishing/finishing, the tool path can form a closed loop, and the tool path is smooth and consistent, which can improve machining efficiency. At

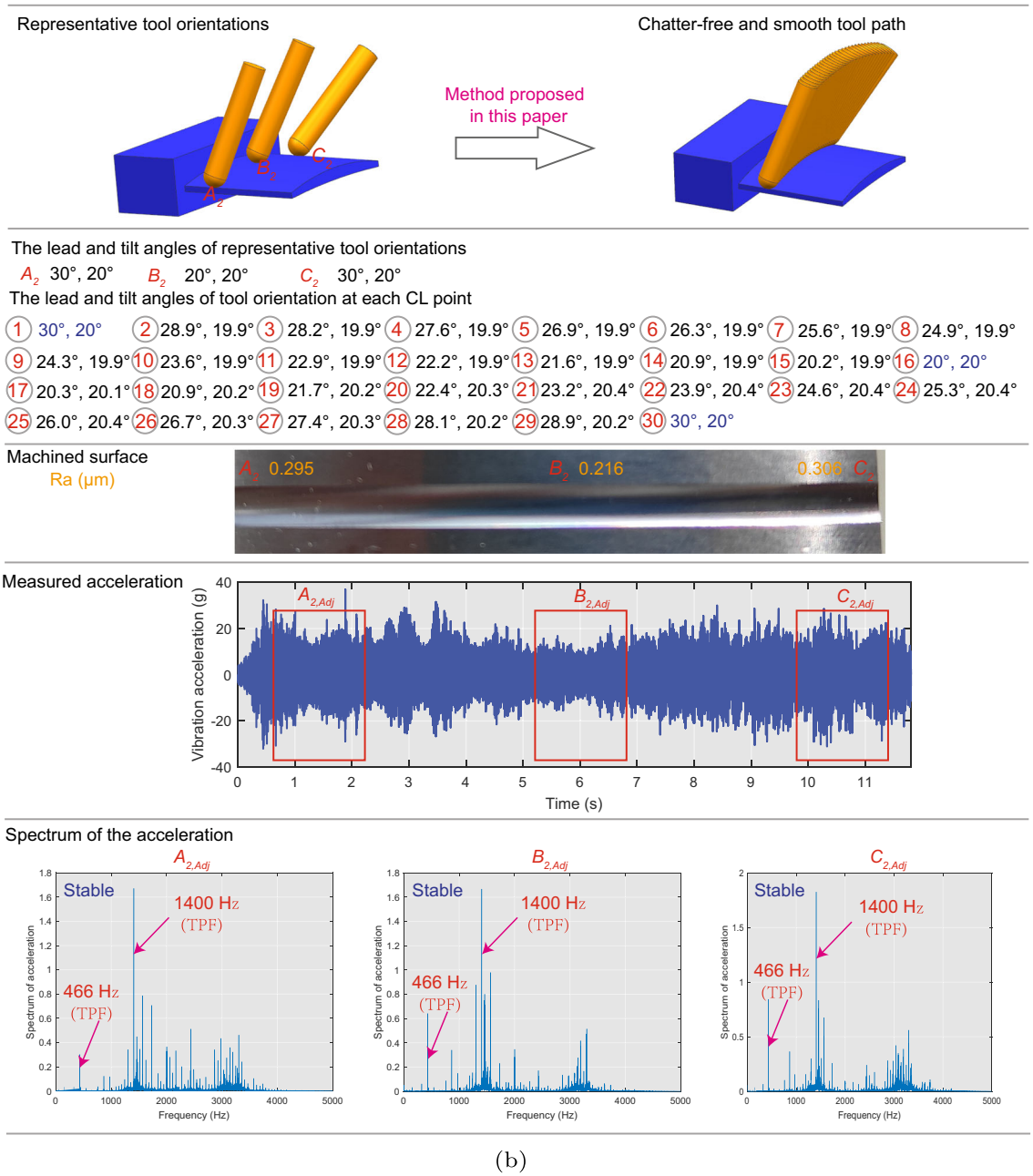

(b)

Fig. 16 continued

the same time, the tool path is uniform and the tool path is easy to control.

The 4-fluted ball-end mills with a diameter of 8 mm and a nominal helix angle of 40° were used in the test, the tool overhang $L = 50$ mm. In rough machining, the cutting depth $a_p = 0.6$ mm, the rotation speed $n = 3000$ rpm, the feed speed $f = 360$ mm/min. In semi-finishing, the cutting depth $a_p = 0.4$ mm, the transverse feed $a_f = 0.2$ mm, the rotation speed $n = 6500$ rpm, and the feed speed $f = 760$ mm/min. In finishing machining, the cutting depth $a_p = 0.1$ mm, the transverse feed $a_f = 0.1$ mm, the rotation speed $n = 7670$ rpm, and the feed speed $f = 760$ mm/min. In order to show the effectiveness of the proposed method, the tool orientation of $\alpha = 10°$, $\beta = 10°$, and the optimized tool orientations as shown in Fig. 17d were used for milling.

Due to the limitations of experimental conditions, a contact acceleration sensor was used to measure the vibration acceleration signal during the cutting process. Since the

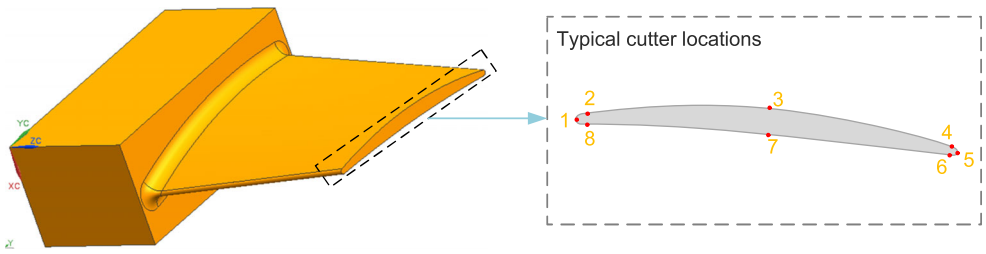

(a)

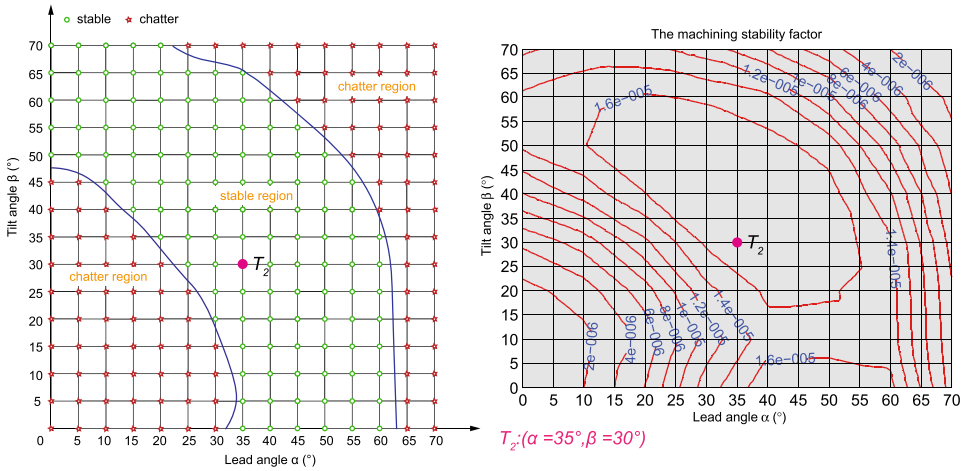

(b)

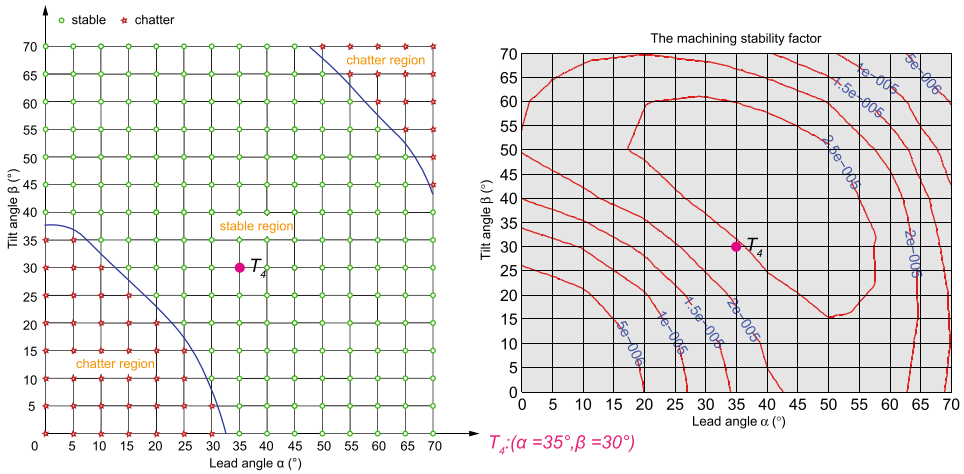

(c)

Fig. 17 Milling of thin-wall blade: **a** typical CL points, **b** stable tool orientation region and machining stability factors at CL point 2, **c** Stable tool orientation region and machining stability factors at CL point 4; **d** chatter-free and smooth tool orientations generated by the proposed method

workpiece was rotating with the workbench during the machining process, the acceleration sensor was fixed on the stator of the spindle to measure the vibration acceleration during the machining process. However, due to the small cutting amount during the finishing process, the cutting vibration amplitude at the location of the acceleration sensor was small, and coupled with the influence of external interference signals, the measured acceleration signal data was poor, so the measurement is not presented. The surface morphology and surface roughness of the machined workpiece are used to analyze the difference in results obtained by machining with unoptimized tool orientation and optimized tool orientation. The mobile roughness measuring instrument Masurf M300C was used to measure the surface roughness of blades.

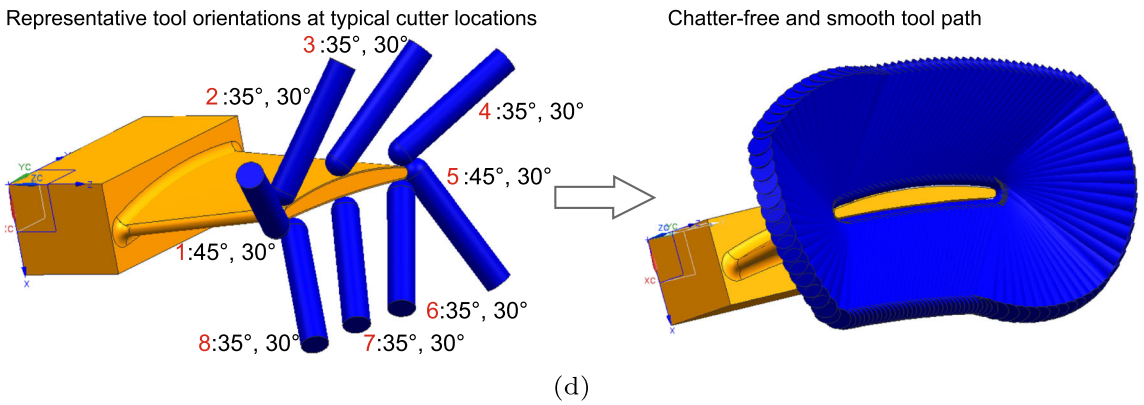

Fig. 17 continued

For each area, measurements were repeated three times and the average value was calculated.

The surface morphology of the workpiece machined by different tool orientations is shown in Fig. 18. For workpiece 1, the tool orientation is $\alpha = 10°$ and $\beta = 10°$, there are obvious vibration marks on the machined surface of the blade tip part. The optimized tool orientations were used to machine workpiece 2, and the blade surface transition is smooth and there are no chatter marks. The measured surface roughness of the area $A1$ on workpieces 1 is 1.253 μm. The measured surface roughness of the area $A2$ on workpiece 2 is 0.447 μm. The above results show that for the tip part of blade, the unoptimized tool orientation causes chatter and result in poor surface quality; while the process is stale for the machining with optimized tool orientation, and the surface quality is better. The vibration suppression strategy based on tool orientation optimization proposed in this article can effectively suppress the cutting chatter during the milling process of thin-walled blades and improve the surface quality of thin-walled blades.

6 Conclusions

A process mechanics based method is presented to generate chatter-free and smooth tool orientations for milling curved thin-walled parts. Firstly, a coupling dynamic model considering both the flexible tool and workpiece is presented in the TCS, the model can predict the cutting stability of the entire process of milling thin-walled parts. Then, a binary search algorithm based single-frequency method is presented to calculate limiting cutting depth. The method does not rely on the initial cutting depth and the increment of cutting depth which selected for calculation, the proposed method can expedite the convergence process for calculating the limiting cutting depth. In addition, an iteratively strategy of first generating smooth tool orientation through the RTOs at the typical locations, and then checking the machining stability and adjusting tool orientation is proposed to generate chatter-free tool orientations along tool path. During this process, a machining stability factor is presented as a criterion to select tool orientation, and the tool orientations have higher value of stability

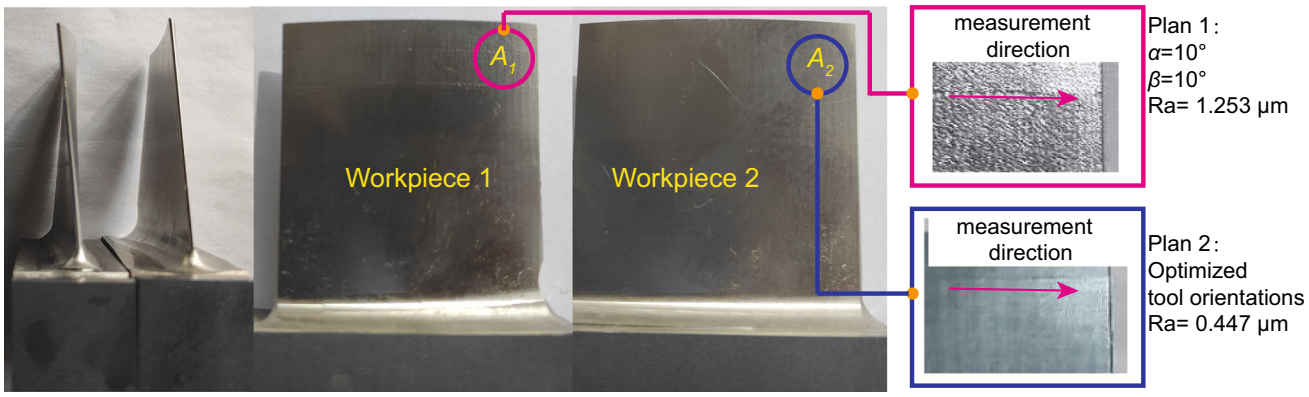

Fig. 18 Comparison of surface morphology of thin-walled blades machined by different tool orientations

factor are selected as the RTOs. The proposed method only needs to obtain the chatter-free tool orientation regions at typical CL point. Moreover, for the thin-walled part studied in this paper, the proposed method can generate the chatter-free tool orientations without iterative calculation, the calculation process is rapid. The simulations and milling tests performed on both block workpiece and curved thin-walled part indicate that the proposed method can effectively generate chatter-free and smooth tool orientations, and improve the quality of machined surface.

7 Appendix

$$\boldsymbol{R}(\boldsymbol{C},\alpha)=\begin{bmatrix} c_i^2+(1-c_i^2)C(\alpha) & c_ic_jV(\alpha)+c_kS(\alpha) & c_ic_kV(\alpha)-c_kS(\alpha) \\ c_ic_jV(\alpha)-c_kS(\alpha) & c_j^2+(1-c_j^2)C(\alpha) & c_jc_kV(\alpha)+c_iS(\alpha) \\ c_ic_kV(\alpha)+c_kS(\alpha) & c_jc_kV(\alpha)-c_iS(\alpha) & c_k^2+(1-c_k^2)C(\alpha) \end{bmatrix} \tag{A1}$$

where $C(\alpha)=\cos(\alpha)$, $S(\alpha)=\sin(\alpha)$, $V(\alpha)=1-\cos(\alpha)$, $\boldsymbol{C}=[c_i,c_j,c_k]^T$.

$$\boldsymbol{R}(\boldsymbol{F},\beta)=\begin{bmatrix} f_i^2+(1-f_i^2)C(\beta) & f_if_jV(\beta)+f_kS(\beta) & f_if_kV(\beta)-f_kS(\beta) \\ f_if_jV(\beta)-f_kS(\beta) & f_j^2+(1-f_j^2)C(\beta) & f_jf_kV(\beta)+f_iS(\beta) \\ f_if_kV(\beta)+f_kS(\beta) & f_jf_kV(\beta)-f_iS(\beta) & f_k^2+(1-f_k^2)C(\beta) \end{bmatrix} \tag{A2}$$

where $C(\beta)=\cos(\beta)$, $S(\beta)=\sin(\beta)$, $V(\beta)=1-\cos(\beta)$, $\boldsymbol{F}=[f_i,f_j,f_k]^T$.

Acknowledgements This work was supported by the National Natural Science Foundation of China (Grant No. 52075451), the National Science and Technology Major Project (J2019-VII-0001-0141).

Author Contribution All authors contributed to the design and implementation of the concept. Dazhen Wang: methodology, algorithm design, data processing, writing manuscript; Weijun Tian: experimental design, data collection; Jinhua Zhou: data analysis; Junxue Ren: conceptualization. The manuscript was written by Dazhen Wang and all authors commented on of the manuscript.

Funding This work received financial support from the National Natural Science Foundation of China (Grant No. 52075451), the National Science and Technology Major Project (J2019-VII-0001-0141). Adding a funding project: the project funded by Shaanxi Provincial Department of Science and Technology (S2024-JC-YB-1396).

Declarations

Competing of Interest The authors declare no competing interests.

References

1. Lasemi A, Xue D, Gu P (2010) Recent development in CNC machining of freeform surfaces: a state-of-the-art review. Comput Aided Des 42(7):641–654. https://doi.org/10.1016/j.cad.2010.04.002
2. Liang F, Kang C, Fang F (2021) A review on tool orientation planning in multi-axis machining. Int J Prod Res 59(18):5690–5720. https://doi.org/10.1080/00207543.2020.1786187
3. Kiswanto G, Hendriko H, Duc E (2014) An analytical method for obtaining cutter workpiece engagement during a semi-finish in five-axis milling. Comput Aided Des 55:81–93. https://doi.org/10.1016/j.cad.2014.05.003
4. Ozturk E, Tunc LT, Budak E (2009) Investigation of lead and tilt angle effects in 5-axis ball-end milling processes. Int J Mach Tools Manuf 49(14):1053–1062. https://doi.org/10.1016/j.ijmachtools.2009.07.013
5. Zhan D, Jiang S, Niu J, Sun Y (2020) Dynamics modeling and stability analysis of five-axis ball-end milling system with variable pitch tools. Int J Mechl Sci 182:105774. https://doi.org/10.1016/j.ijmecsci.2020.105774
6. Tang X, Peng F, Yan R, Zhu Z, Li Z, Xin S (2020) Nonlinear process damping identification using finite amplitude stability and the influence analysis on five-axis milling stability. Int J Mechl Sci 190:106008. https://doi.org/10.1016/j.ijmecsci.2020.106008
7. Tang X, Zhu Z, Yan R, Chen C, Peng F, Zhang M, Li Y (2018) Stability prediction based effect analysis of tool orientation on machining efficiency for five-axis bull-nose end milling. J Manuf Sci Eng 140(12):121015. https://doi.org/10.1115/1.4041426
8. Falta J, Sulitka M, Zeman P (2022) An analytical formulation of zoa-based machining stability for complex tool geometries: application to 5-axis ball-end milling. Int J Adv Manuf Technol 123(5–6):1499–1519
9. Budak E, Ozturk E, Tunc L (2009) Modeling and simulation of 5-axis milling processes. CIRP annals 58(1):347–350. https://doi.org/10.1016/j.cirp.2009.03.044
10. Ozturk E, Budak E (2010) Dynamics and stability of five-axis ball-end milling. J Manuf Sci Eng 132(2):021003. https://doi.org/10.1115/1.4001038
11. Ma J, Zhang D, Liu Y, Wu B, Luo M (2017) Tool posture dependent chatter suppression in five-axis milling of thin-walled workpiece with ball-end cutter. Int J Adv Manuf Technol 91(1–4):287–299. https://doi.org/10.1007/s00170-016-9748-0
12. Li Z, Yan R, Tang X, Peng F, Xin S, Wu J (2021) Analysis of the effect of tool posture on stability considering the nonlinear dynamic cutting force coefficient. J Manuf Sci Eng 143(8):081009
13. Cai Y, Zhang Z, Xi X, Zhao D (2023) A deformation control method in thin-walled parts machining based on force and stiffness matching via cutter orientation optimization. J Manuf Sci Eng 145(3):031007
14. Zhang X, Zhang J, Zheng X, Pang B, Zhao W (2017) Tool orientation optimization of 5-axis ball-end milling based on an accurate cutter/workpiece engagement model. CIRP J Manuf Sci Technol 19:106–116. https://doi.org/10.1016/j.cirpj.2017.06.003
15. Yigit IE, Lazoglu I et al (2015) Analysis of tool orientation for 5-axis ball-end milling of flexible parts. CIRP Annals 64(1):97–100. https://doi.org/10.1016/j.cirp.2015.04.067
16. Munoa J, Beudaert X, Dombovari Z, Altintas Y, Budak E, Brecher C, Stepan G (2016) Chatter suppression techniques in metal cutting. CIRP Annals 65(2):785–808. https://doi.org/10.1016/j.cirp.2016.06.004
17. Tunc LT, Budak E, Bilgen S, Zatarain M (2016) Process simulation integrated tool axis selection for 5-axis tool path generation. CIRP Annals 65(1):381–384. https://doi.org/10.1016/j.cirp.2016.04.113
18. Wang S, Geng L, Zhang Y, Liu K, Ng T (2016) Chatter-free cutter postures in five-axis machining. Proc Inst Mechl Eng, Part B: J Eng Manuf 230(8):1428–1439. https://doi.org/10.1177/0954405415615761

19. Sun C, Altintas Y (2016) Chatter free tool orientations in 5-axis ball-end milling. Int J Mach Tools Manuf 106:89–97. https://doi.org/10.1016/j.ijmachtools.2016.04.007
20. Zhao Z, Wang S, Wang Z, Liu N, Wang S, Ma C, Yang B (2020) Interference-and chatter-free cutter posture optimization towards minimal surface roughness in five-axis machining. Int J Mech Sci 171:105395. https://doi.org/10.1016/j.ijmecsci.2019.105395
21. Huang T, Zhang X-M, Leopold J, Ding H (2018) Tool orientation planning in milling with process dynamic constraints: a minimax optimization approach. J Manuf Sci Eng 140(11):111002. https://doi.org/10.1115/1.4040872
22. Karimi B, Altintas Y (2024) Chatter avoidance by spindle speed and orientation planning in five-axis ball-end milling of thin-walled blades. J Manuf Sci Eng 146(2)
23. Wan M, Wang Y-T, Zhang W-H, Yang Y, Dang J-W (2011) Prediction of chatter stability for multiple-delay milling system under different cutting force models. Int J Mach Tools Manuf 51(4):281–295. https://doi.org/10.1016/j.ijmachtools.2010.12.007
24. Zhang Z, Li H, Liu X, Zhang W, Meng G (2018) Chatter mitigation for the milling of thin-walled workpiece. Int J Mech Sci 138:262–271. https://doi.org/10.1016/j.ijmecsci.2018.02.014
25. Budak E, Altintas Y (1998) Analytical prediction of chatter stability in milling. Part I: general formulation. ASME Journal of Dynamic Systems, Measurement, and Control 120(1):22–30. https://doi.org/10.1115/1.2801317
26. Wang D, Ren J, Tian W (2020) A method for the prediction of cutting force for 5-axis ball-end milling of workpieces with curved surfaces. Int J Adv Manuf Technol 107(5–6):2023–2039. https://doi.org/10.1007/s00170-020-05030-5
27. Altintas Y (2012) Manufacturing automation: metal cutting mechanics, machine tool vibrations, and CNC design, pp 138. Cambridge University Press, UK
28. Ho M-C, Hwang Y-R, Hu C-H (2003) Five-axis tool orientation smoothing using quaternion interpolation algorithm. Int J Mach Tools Manuf 43(12):1259–1267. https://doi.org/10.1016/S0890-6955(03)00107-X
29. Yuan Y-x (2008) Step-sizes for the gradient method. AMS IP Studies in Advanced Mathematics 42(2):785–796
30. Wang D, Ren J, Tian W, Shi K, Zhang B (2019) Predicting the dynamics of thin-walled parts with curved surfaces in milling based on fem and Taylor series. Int J Adv Manuf Technol 103(1–4):927–942. https://doi.org/10.1007/s00170-019-03585-6

Authors and Affiliations

Wang Dazhen[1,2] · Tian Weijun[3] · Zhou Jinhua[2] · Ren Junxue[2]

✉ Wang Dazhen
wangdazhen@mail.nwpu.edu.cn

Tian Weijun
2692298564@qq.com

Zhou Jinhua
1542426851@qq.com

Ren Junxue
1732768135@qq.com

[1] Xi'an Aerospace Propulsion Testing Technology Research Institute, 137 Tianhongzheng Street, Xi'an 710025, Shaanxi, China

[2] School of Mechanical Engineering, Northwestern Polytechnical University, 127 West Youyi Road, Xi'an 710072, Shaanxi, China

[3] Training Center for Engineering Practices, Northwestern Polytechnical University, 1 Dongxiang Road, Xi'an 710129, Shaanxi, China